

PHOTOMULTIPLIER TUBE PARAMETERS
FOR MEASUREMENT OF LOW LIGHT LEVELS

by 632

JOHN HENRY BRAND II

B. S., Kansas State University, 1968

A MASTER'S THESIS

submitted in partial fulfillment of the

requirements for the degree


MASTER OF SCIENCE

Department of Physics

KANSAS STATE UNIVERSITY
Manhattan, Kansas

1970

Approved by:


Major Professor

LD
2668
T4
1970
0722
C.2

TABLE OF CONTENTS

Introduction	1
General Discussion of Photomultipliers	2
Pulse Height Distributions	9
Theory of Pulse Height Spectra	13
Experimental Apparatus and Techniques	25
Data Reduction	31
Results and Conclusions	40
Appendix	93
Acknowledgments	98
References	99

ILLEGIBLE DOCUMENT

**THE FOLLOWING
DOCUMENT(S) IS OF
POOR LEGIBILITY IN
THE ORIGINAL**

**THIS IS THE BEST
COPY AVAILABLE**

**THIS BOOK
CONTAINS
NUMEROUS
PAGES THAT ARE
CUT OFF**

**THIS IS AS
RECEIVED FROM
THE CUSTOMER**

**THIS BOOK
CONTAINS
NUMEROUS PAGES
WITH DIAGRAMS
THAT ARE CROOKED
COMPARED TO THE
REST OF THE
INFORMATION ON
THE PAGE.**

**THIS IS AS
RECEIVED FROM
CUSTOMER.**

INTRODUCTION

A photomultiplier is a device which yields a pulse of charge as output a certain fraction of the time upon receiving an input light signal. The output signal varies statistically in size. In addition, output pulses are obtained even with no light input; these noise pulses follow statistical rules also.

Ordinary pulse counting measurements, possible when output pulses from all sources can be individually discerned, blindly add up pulses as they come in, regardless of pulse origin. In dc measurements there is a dc component of signal representing the time-averaged charge output, contaminated by an ac component which represents ac noise generated in resistors and the ac component of the output pulses. The signal-to-noise expressions for dc measurements (involving dc or ac measurements) are difficult to obtain and still provide no information to use in rejecting pulses which, on the average, look like signal pulses yet do not arise from signal.

From the above it is evident that, if output pulses are sparse enough so that the individual pulses can be resolved in time, a means of rejecting non-signal pulses would improve both the pulse counting and dc methods of measurement of weak light sources with photomultiplier tubes. This study was undertaken to identify the relevant parameters affecting signal-to-noise ratios and to determine the best values of the parameters for several particular tubes.

GENERAL DISCUSSION OF PHOTOMULTIPLIERS

In a light detector three things are desired: (1) sensitivity to very small signals; (2) high signal-to-noise ratio; (3) output directly proportional to light intensity input. In the visible and near-visible regions of the electromagnetic spectrum the photomultiplier suits this purpose well. The photomultiplier consists of a material that emits electrons upon absorption of light energy, followed by a series of dynodes at decreasing potential with respect to each other. The photoelectron is accelerated by the interdynode potential to the first dynode, where it causes the emission of secondary electrons. The number of secondary electrons follows a probability law. The resulting secondary electrons are then accelerated to the second dynode, where more secondary electrons are emitted and the cascade continues, as shown in Plate I^{1,2}. The same number of secondary electrons is unlikely to be emitted each time an incident electron impinges on a dynode surface. Consequently, dependent upon chance, a statistical distribution of sizes of output pulses is to be expected.

Many things can happen to mask this distribution. There is always some ohmic leakage between dynode structures; even glass insulators have finite conductivity. Thermal electrons emitted at various stages in the amplification process behave like photoelectrons, starting cascades that have the same form, assuming uniform dynode properties, as cascades due to photoelectrons, though of smaller average net charge. In dc measurements, one must worry about Schottky noise and Johnson noise. Schottky noise is due to the fact that the electrons in a steady current flow pass a point randomly in time. Johnson noise reflects the fact that random thermal motion of electrons in the load resistor generates white noise³. There are also the possibilities of ion feedback, prepulsing, afterpulsing, natural radioactivity,

EXPLANATION OF PLATE I

Two of the most widely used types of photomultipliers.

Fig. 1: Venetian blind type.

Fig. 2: Compact type.

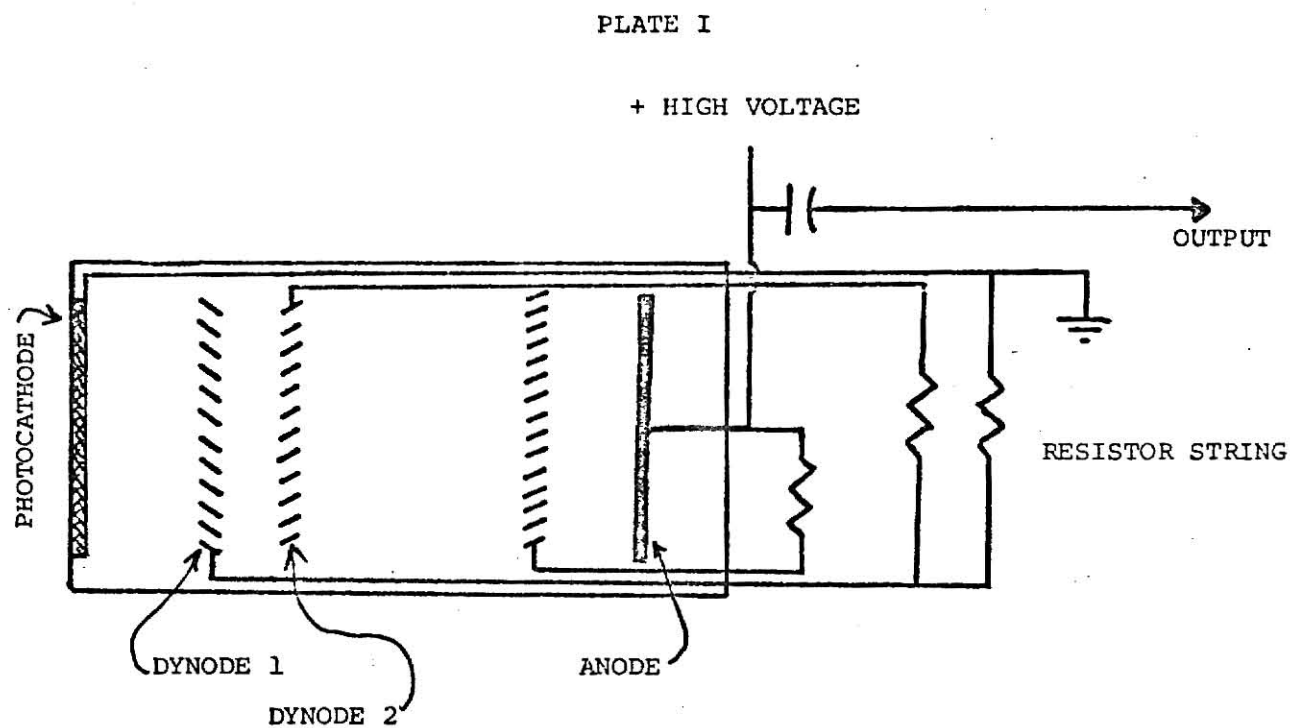


Figure 1.

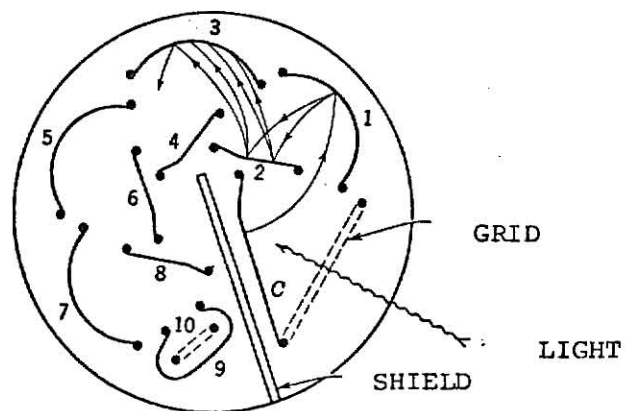


Figure 2.

and fluorescence, some or all of which can make a tube unsuitable for either ac or dc work. Ion feedback, prepulsing, afterpulsing, and fluorescence can be eliminated by careful design, and it is thought that the extremely large pulses found in some tubes and which do not abate at low temperatures are due to natural radioactivity of the glass and metal of the tube^{4,5,6}. These pulses can be eliminated by use of an upper level discriminator, once their origin is determined.

With all of these faults, it may be wondered why the photomultiplier is used instead of a Golay cell, or thermistor, or even a phototube with electronic instead of cascade amplification. The first two are unsuitable because of lack of sensitivity and long response time. The photomultiplier anode can be considered to be a capacitor which receives a packet of charge in a time interval of about a nanosecond and which subsequently discharges through a load resistor. For a 1P21 photomultiplier tube with capacitance ~ 6 pF, a rise time of ~ 2 nsec has been observed⁷. Discharge through a $1\text{M}\Omega$ load resistor would give rise to a decay time of about $6 \mu\text{s}$. Some special photomultipliers have even sharper pulses.

Let us compute the advantage of multiplier amplification over an electronic amplifier⁸. Consider a photocell with an electronic amplifier of band width Δf and a photomultiplier with load resistor R and anode current I_0 . Let the photomultiplier tube have an ideal multiplier, with a photocathode of well-defined quantum efficiency. This tube can detect a minimum luminous flux of ϕ_m . Let the photocell have the same photocathode. For the photocell and the electronic amplifier let the minimum detectable luminous flux be ϕ_v . The gain in signal of the multiplier over the amplifier is

$$G = \frac{\phi_v}{\phi_m} .$$

Assume that the output of the multiplier needs no further electronic amplification and that gain fluctuations due to secondary emission are negligible compared to the Schottky noise. This is true if the multiplication at the first dynode is greater than 2. If this is so, the photocathode yields a current I_o , the mean square noise component of which is³

$$\langle i^2 \rangle = 2e I_o \Delta f .$$

Since the measurement is dc, thermionic emission and background flux can be considered a steady, dc source of noise. Introduce a modulation factor Γ defined for the photocathode such that

$$\Gamma \equiv \sqrt{2} \frac{I_m}{I_o} ,$$

where I_m is the photoelectric current containing the information of interest. Assume the current of interest must have a signal-to-noise ratio ρ in order to be detectable. Then,

$$I_m = \rho \sqrt{2e I_o \Delta f} .$$

If the signal is multiplied by an ideal electronic amplifier, the noise comes from Johnson noise in the amplifier input resistor:

$$\langle v^2 \rangle = 4kTR\Delta f .$$

For the electronic amplifier, the photocathode current must have the value

$$I_v = \rho \sqrt{\frac{4kT\Delta f}{R}} .$$

If C is the input capacitance of the amplifier,

$$\Delta f \approx \frac{1}{2\pi RC},$$

RC being the time constant of the amplifier-detector system. Then,

$$G = \frac{I_{\nu}}{I_M} = \frac{\Gamma}{e\rho} \sqrt{\pi kTC} = 7 \times 10^8 \frac{\Gamma}{\rho} \sqrt{C}$$

at room temperature, C being expressed in farads. If $C = 20 \mu\mu F$ and $\rho = 2$, then

$$G = 1600 \Gamma.$$

If Γ equals 1; that is, if no stray light hits the tube and there is no dark current in the tube, the multiplier can detect a signal 1600 times weaker than a photocell plus amplifier⁸.

In pulse counting applications, the minimum detectable signal is usually considered to be "equal to the statistical uncertainty in the dark count"⁹. It has been shown, however, that electron pulse counting has a greater signal-to-noise ratio than dc methods¹⁰. Indeed, for applications such as the beam-foil technique, where the source is extremely faint, the advantage of pulse counting (with a quiet tube) over lock-in amplification is about four to one in minimum detectable flux. Two dc methods of detecting a very weak signal were opposed to pulse counting for a weak Raman line. The dc methods were lock-in amplification and the "noise-voltage technique", a method in which the shot noise of the photocathode is observed. Three detection systems were constructed and the three methods tried in turn. The pulse counting technique could detect a minimum of two counts/sec or 1.3×10^{-17} W input power. The lock-in amplification method could detect a minimum

of 5.7×10^{-17} W or 4.4 times the minimum detectable signal of the pulse counting technique; the noise-voltage method could detect a minimum of 4×10^{-17} W or 3.1 times the minimum detectable signal of the pulse counting technique.

Consequently, if one desires to eliminate unwanted noise pulses, it behooves one to have some idea of what the pulse height distribution from a photomultiplier looks like, and where in the multiplier the pulses from some given part of that distribution most likely had their origin. This is also important to nuclear physicists, who wish to know what an "ideal line" from their scintillation counters looks like.

PULSE HEIGHT DISTRIBUTIONS

There has been in the past some disagreement over which photomultipliers produced what shape of single electron pulse height spectrum. The ideal case would be a pulse height spectrum with clearly defined peaks corresponding to single electrons, electron pairs, triplets, and so on, being emitted from the photocathode and cascading down the multiplier assembly as shown in Fig. 1.

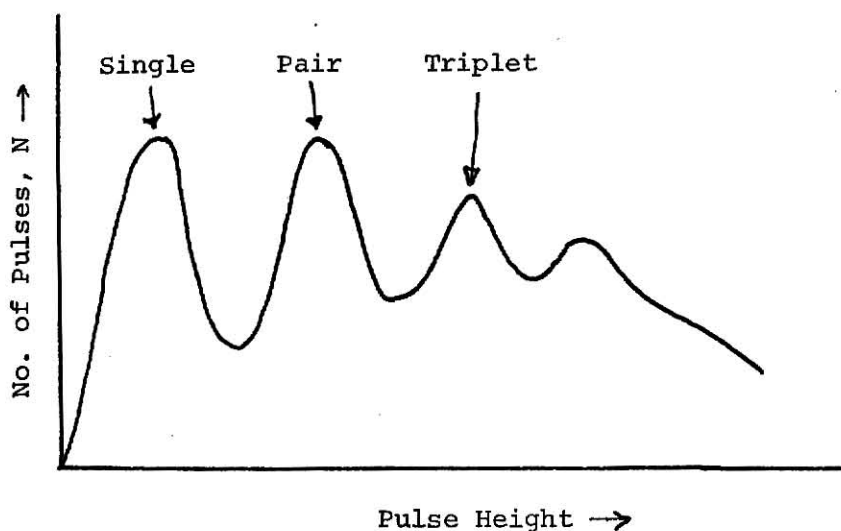


Fig. 1, Multiple Peak Pulse Height Distribution (A)

In recent years a distribution very like this has indeed been observed¹¹. More often, however, pulse height spectra similar to Fig. 2^{12,13} have been obtained.

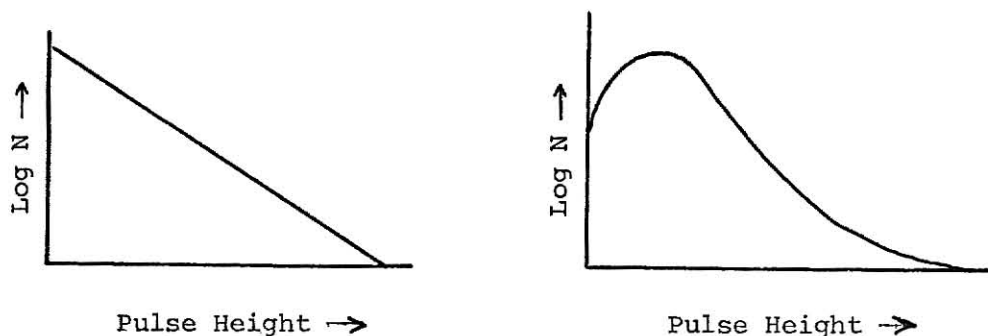


Fig. 2, Exponential and Peaked Distributions (B,C)

In other cases the pulse height distribution may look like Fig. 3⁴.

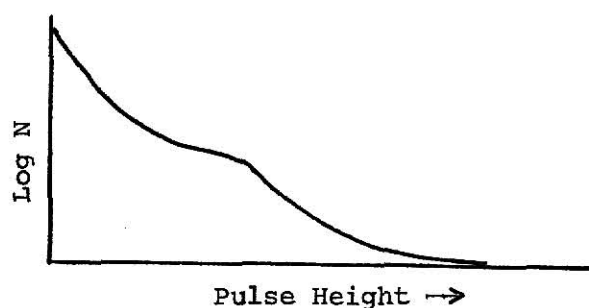


Fig. 3, Quasi-Exponential Pulse Height Distribution (D)

Case (B) suggests an exponential or Furry probability in the distribution function for one cascade; case (C) suggests a Poisson distribution, and (D) suggests multiple parallel processes of electron multiplication. Case (D) is usually obtained when all sections of the distribution are not affected equally by temperature. One obvious way to surmount part of the dark noise problem due to thermionic emission is to cool the tube; Engstrom showed that for the 1P21 family of photomultipliers the dark current follows at least approximately Richardson's equation down to low temperatures, where a low temperature tail is observed. The deviations from a Richardson's curve were ascribed to different values of the work function in the tube¹⁴. The low temperature deviation is now ascribed to cosmic rays and radioactivity of the tube and environs producing multiple photon events¹⁵. In many photomultipliers, if not most, there is a distinct high energy tail to the pulse height distribution.

The exact shape of the cascade distribution is important, since, if the information on the origin of the electron cascade is not destroyed by the statistics, a discriminator, or "window", can be set to eliminate unwanted signal that probably does not originate from the photocathode. It is difficult to discriminate between single thermal and photoelectrons from the cathode, as the difference between the two, if any, in initial

velocities on leaving the surface of the cathode is overwhelmed in the common acceleration across a potential of the order of a hundred volts for electrons of all sources. Nevertheless, there is considerable advantage to be had in measuring only electrons originating from the cathode, as a considerable amount of noise is still eliminated.

There are two fairly simple rationalizations for the two types of single electron spectrum usually claimed. As a simple, probably invalid model, the exponential distribution can be imagined to arise from raising the temperature of the electron gas in the region of the primary electron impact so that the distribution of electron energies goes from a sharp cutoff to a slightly less sharp cutoff, Fig. 4.

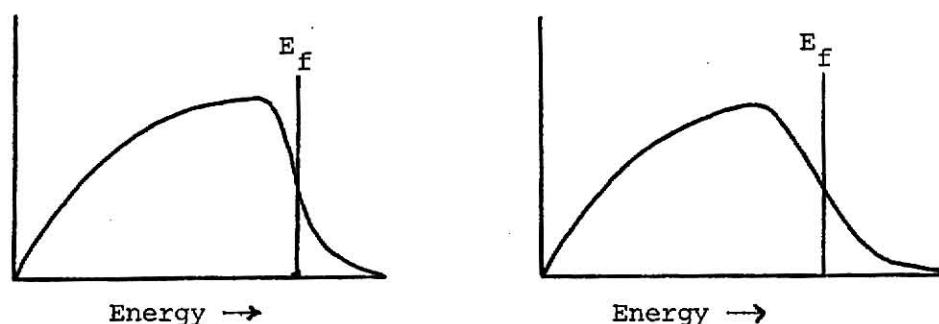


Fig. 4, Population vs Energy Distributions

If we assume an electron escapes from the solid by undergoing numerous collisions and finally wandering out of the material, the higher energy electrons are able to wander longer and still overcome the work function at the surface. There might then be an approximately exponential population distribution of secondary electrons¹⁶. Another argument is that an electron splashing out another electron is essentially a go, no-go proposition or Bernoulli process. Thus there is, for a given occurrence, a certain probability ρ of an electron-electron collision producing the

desired result. This would give rise to a binomial probability distribution; if the number of collisions becomes large and the probability of electron escape small, we have a Poisson distribution resulting.

THEORY OF PULSE HEIGHT SPECTRA

There are two general ways of measuring the single electron pulse height distribution. One way is to run one's tube with a very weak light source of known frequency incident on the photocathode and then subtract the dark current pulse height distribution from the distribution resulting from the light and dark noise pulses, the light counts and dark counts together being sufficiently small in number that the tube multiplication parameters do not change and pulse pile up does not occur.

A number of authors have reported single electron spectra with peaked distributions^{12,17-22} and a like number with exponential or quasi-exponential distributions^{5,13,14,18,23-34}. Efforts have been made to calculate probability distributions based on either exponential or Poisson statistics; these have met with varying success^{12,21,35,36}. The situation was clarified somewhat when Delaney and Walton showed that, for some tube configurations, light could pass the photocathode, reach the dynode structure, and contaminate the observed pulse height spectrum with single electron pulse height spectra from dynodes 1, 2, and so on. With this caveat, they were able to obtain from some tubes single photoelectron pulse height spectra which were clearly based on Poisson statistics. Nevertheless, with some tubes they could not obtain the desired peaked spectra¹⁸.

Prescott (1966) attempted a model of the single electron multiplication process using the same general procedure as previous workers, except that, instead of an exponential or Poisson distribution, he assumed a Polya probability distribution:

$$P(x) = \frac{\mu^x}{x!} \left(1 + \frac{1}{b}\mu\right)^{-x-1/b} \prod_{\xi=1}^{x-1} (1 - \xi/b),$$

where μ is the mean of the distribution, and b is a "shaping parameter"³⁷. When $b = 1$, this distribution is the quasi-exponential, or Furry distribution; when $b = 0$, the distribution becomes the Poisson distribution. The Polya distribution is also known as the "negative binomial distribution" or "compound Poisson" distribution.

Using the generating function $G(s)$ of a probability function $f(x)$, let us develop an interpretation of the Polya distribution and an iteration formula for the problem of a secondary electron cascade. Let $f(x)$ be the frequency function for x secondaries for each stage of multiplication; then

$$G(s) = \sum_{\text{all } x} s^x f(x).$$

$G(s)$, where s is an auxiliary variable, is the generating function for $f(x)$.

For the Polya distribution the generating function $G(s)$ is

$$G(s) = \{1 + b\mu(1-s)\}^{-1/b}.$$

The generating function $G_k(s)$ for the output of the k^{th} stage is, then,

$$\begin{aligned} G_k(s) &= G[G\{\dots G(s)\}] \\ &= G[G_{k-1}(s)]. \end{aligned}$$

Through the Polya distribution one may introduce the idea of non-uniform dynodes. Let us assume that the secondary emission distribution is Poissonian, but that the mean of the distribution varies from place to place on each dynode, either because of secondary electron loss or surface variation on the dynode. Let us assume the distribution function for the mean to be $g(m)$. The generating function for a Poisson distribution of mean m is $\exp[m(s-1)]$, so that the generating function for one dynode is

$$G(s) = \int_0^{\infty} g(m) \exp[m(s-1)] dm.$$

Now the moment generating function for m is

$$M_m(s) = \int_0^{\infty} g(m) \exp[ms] dm,$$

so that

$$G(s) = M_m(s-1),$$

and the mean of the compound Poisson distribution is the same as the mean of the mean distribution $g(m)$.

According to Prescott, the relative variance V , where $V \equiv \left[\frac{\text{variance}}{\text{mean}^2} \right]$ is given by

$$V = \frac{1}{\mu} + V_m,$$

where V_m is the relative variance of $g(m)$, and $\frac{1}{\mu}$ is the relative variance of a Poisson distribution of mean μ , so that the relative variance of the compound Poisson distribution is the relative variance of the simple Poisson distribution plus the relative variance of $g(m)$. For the Polya distribution,

$$G(s) = \left[1 + b\mu(1-s) \right]^{-1/b}$$

$$M_m(s) = \left(1 - b\mu s \right)^{-1/b}.$$

By comparison, we may obtain

$$g(m) = \frac{(\mu b)^{-1/b}}{\Gamma(1/b)} m^{(1/b)-1} \exp\left(-\frac{m}{\mu b}\right).$$

We have found that the mean of $g(m)$ is μ ; it is asserted that the variance is $b\mu^2$ and the relative variance b . Except for the exponential case $b = 1$, this distribution $g(m)$ is peaked, with the distribution becoming narrower as $b \rightarrow 0$, $b = 0$ being a delta function $\delta(m - \mu)$. When $b = 0$, the dynodes are perfectly uniform. The pulse height distributions of such dynodes, obeying point Poisson statistics, having a finite area with a mean number of secondaries for the dynode as a whole of μ , with a total probability distribution governed by Polya statistics and a well-defined variance, have a relative variance of $V = \frac{1}{\mu} + b$.

Based on Lombard and Martin's method, assuming equal stage gains and identical dynodes, Prescott obtained theoretical curves for the multiplier structure. We had

$$G_k(s) = G_1[G_{k-1}(s)] \equiv \sum_{\text{all } x} P_k(x) s^x,$$

where $G_k(s)$ is expressed as a Maclaurin series, $P_k(x)$ being the coefficients of the x^{th} power of s . Then

$$P_k(x) = \frac{1}{x!} G_k^{(x)}(s) \Big|_{s=0} = \frac{1}{x!} \left[G_1 \{ G_{k-1}(s) \} \right]^{(x)} \Big|_{s=0},$$

where (x) means x^{th} derivative with respect to s . Applying Leibniz's rule for derivatives:

$$(fg)^{(x)} = \sum_{i=0}^x \binom{x}{i} f^{(i)} g^{(x-i)},$$

and by algebra, we obtain

$$x P_k(x) \left\{ 1 + b\mu [1 - P_{k-1}(0)] \right\} = \mu \sum_{\xi=0}^{x-1} P_k(\xi) P_{k-1}(x-\xi) \left\{ x + \xi(b-1) \right\},$$

$$k \geq 1, x \geq 1,$$

with the initial conditions that

$$P_k(0) = \left\{ 1 + b\mu [1 - P_{k-1}(0)] \right\}^{-1/b};$$

$$\begin{cases} P_0(x) = 1, & x = 1, \\ P_0(x) = 0, & x \neq 1. \end{cases}$$

For completeness, the λ^{th} moment about the origin of the distribution leaving stage K is

$$M_K^{\lambda} = \sum_{x=0}^{\infty} x^{\lambda} P_K(x)$$

$$= \mu M_{K-1}^{\lambda} + \mu \sum_{j=1}^{\lambda-1} \left\{ b \binom{\lambda-1}{j} M_K^{\lambda-j} + \binom{\lambda-1}{j} M_{K-1}^{\lambda-j} M_K^j \right\}.$$

The relative variance V of this same distribution is

$$V = \left(b + \frac{1}{\mu} \right) \left(1 + \frac{1}{\mu} + \frac{1}{\mu^2} + \dots + \frac{1}{\mu^{K-1}} \right).$$

For K large,

$$V = \frac{b\mu + 1}{\mu - 1}.$$

Naturally there will be some cascades that "break"; i.e., at some point all the incident electrons will fail to produce any secondaries at all. Therefore the observed means and variances will differ from the true means and variances.

If k is the fraction that breaks; i.e., $P_k(0)$, then

$$\mu' = \frac{\mu}{1-k}$$

and

$$V' = V(1-k) - k = \frac{[(b\mu+1)(1-k)]}{\mu-1} - k$$

The fractions of chains breaking are given in Table IV.

There are two obvious ways of attempting to fit experimental results to Prescott's work. One can compute the pulse height distributions for a variety of values of μ and b and plot one's experimental data with these distributions, or one can compute the relative variance of one's experimental distribution and compare this against relative variances computed from Prescott's formula using estimated values of b and μ . Programs for computing the variance of the experimental distributions and for computing pulse height distributions using Prescott's iteration formulae are given in the Appendix. Due to the cost of computation only a few distributions were computed. Fortunately the distributions converge to their final shape quickly, five stages of iteration being adequate for $\mu \geq 3$, and four for $\mu \geq 4.5$ ³⁶. It has been observed experimentally that a few stages of amplification determine the shape of the pulse height distributions²⁷, and the distributions calculated display this, as shown in Plates III and IV. Distributions calculated by Prescott for a variety of values of the parameters μ , b are presented in Plate II.

EXPLANATION OF PLATE II

Pulse height distributions for various values of b , the Polya shaping parameter, and μ , the mean interstage gain. Graphs taken from Prescott (1966).

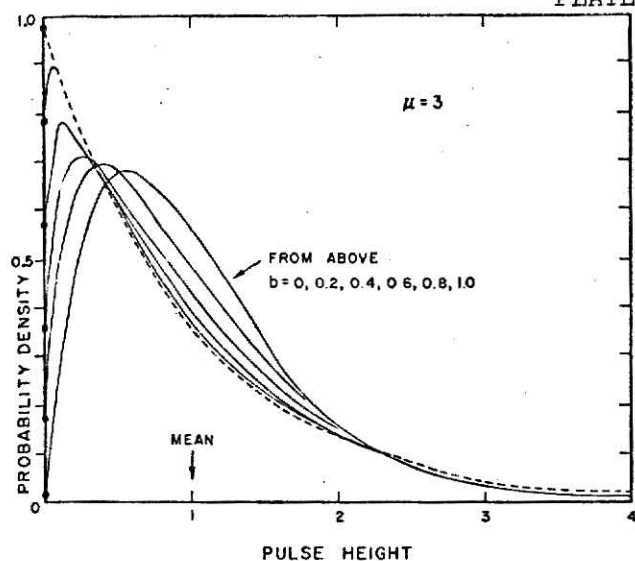


Fig. 1. Computed single-electron distributions at stage-gain 3.0, for a range of values of parameter b .

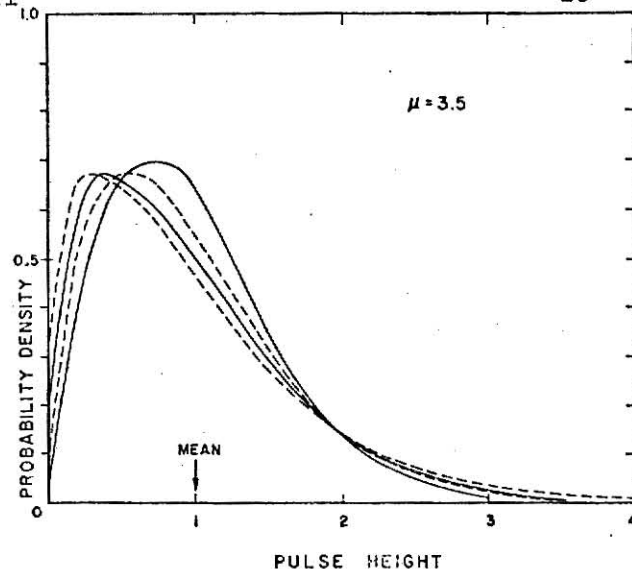


Fig. 2. Computed single-electron distributions at stage-gain 3.5. Parameter b : 0, 0.1, 0.2, 0.3.

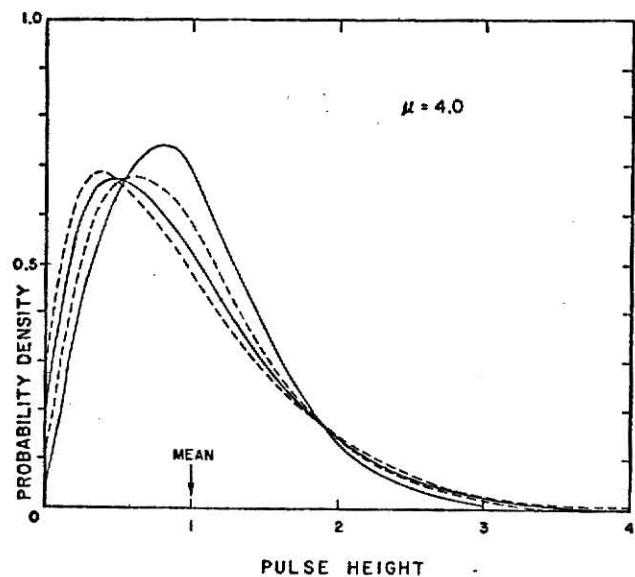


Fig. 3. Computed single-electron distributions at stage-gain 4.0. Parameter b : 0, 0.1, 0.2, 0.3.

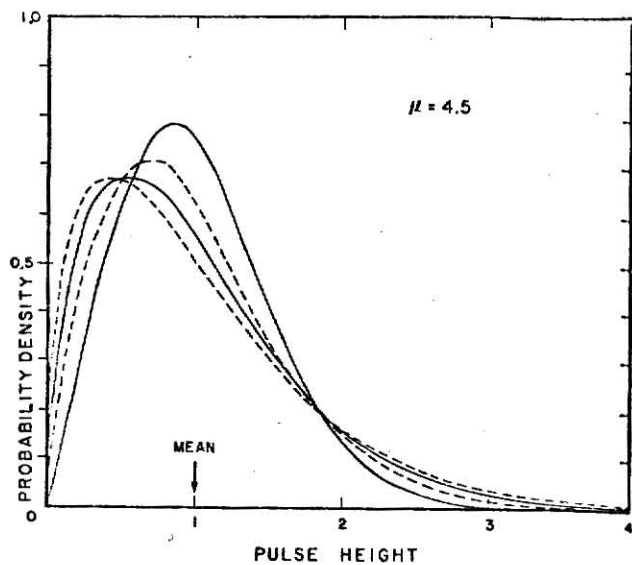


Fig. 4. Computed single-electron distributions at stage-gain 4.5. Parameter b : 0, 0.1, 0.2, 0.3.

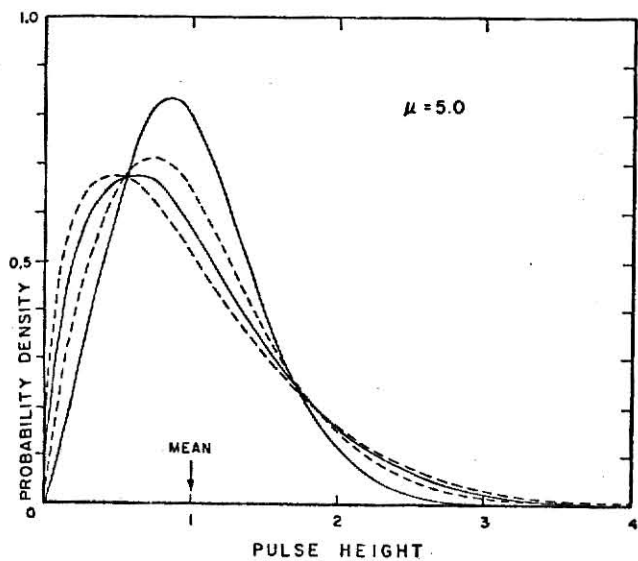


Fig. 5. Computed single-electron distributions at stage-gain 5.0. Parameter b : 0, 0.1, 0.2, 0.3.

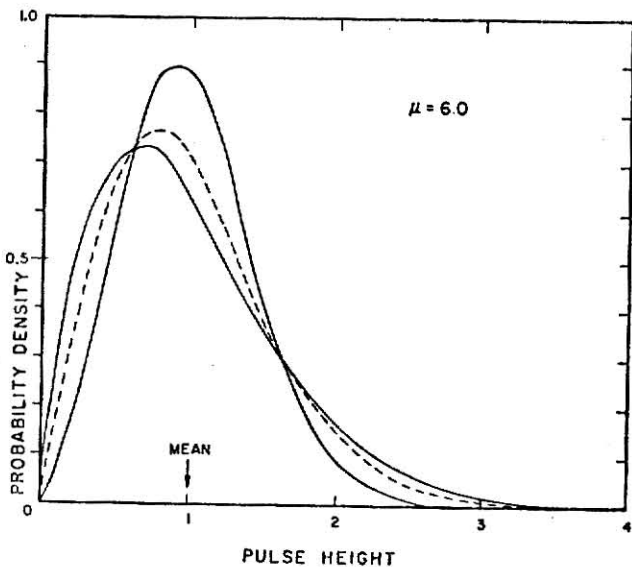
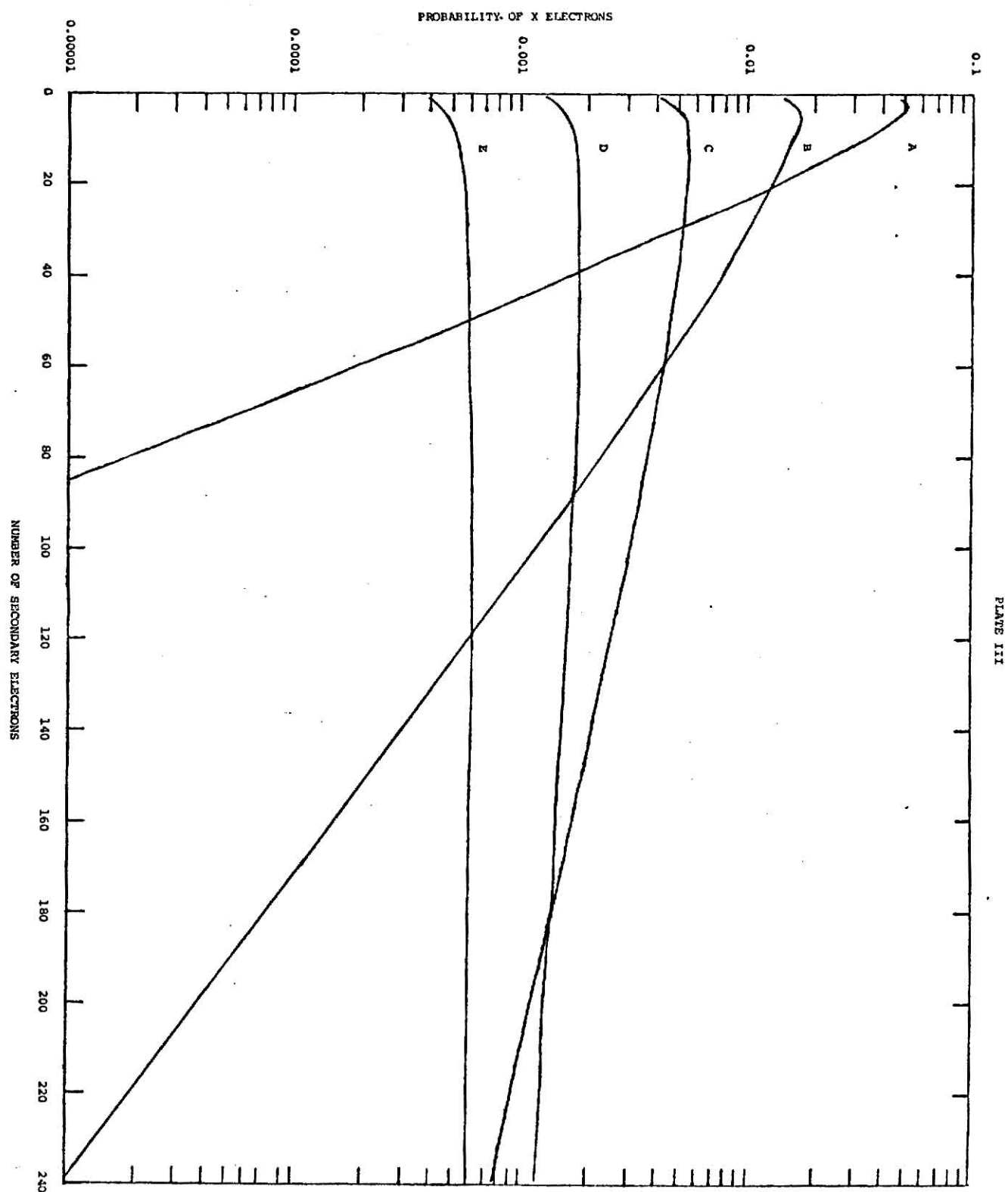


Fig. 6. Computed single-electron distributions at stage-gain 6.0. Parameter b : 0, 0.1, 0.2.

EXPLANATION OF PLATE III

Pulse height distribution for $\mu = 3$, $b = .6$, for different stages of iteration.

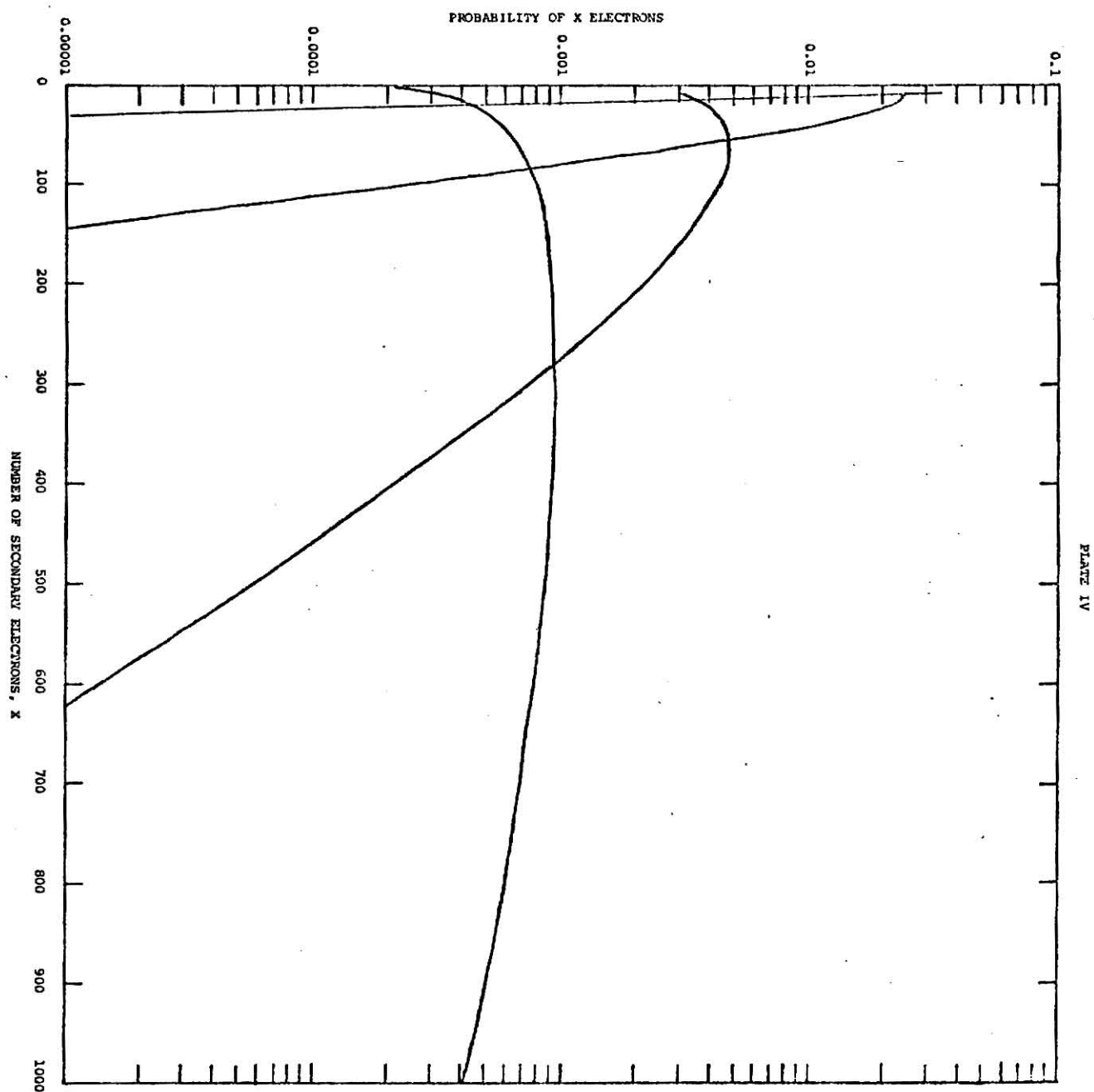
- A. Secondary electron distribution leaving dynode 2.
- B. Secondary electron distribution leaving dynode 3.
- C. Secondary electron distribution leaving dynode 4.
- D. Secondary electron distribution leaving dynode 5.
- E. Secondary electron distribution leaving dynode 6.



EXPLANATION OF PLATE IV

Pulse height distribution for $\mu = 5$, $b = .3$, for different stages of iteration.

The curves, from left to right, represent the secondary electron distributions leaving the first, second, third, and fourth dynodes respectively.



EXPERIMENTAL APPARATUS AND TECHNIQUES

The present measurements were made using a photomultiplier in a light-tight cold box, with the output going into an ND-130 multichannel analyzer or a picoammeter. The temperature control was accomplished by boiling off liquid nitrogen and passing the cold gas through a copper cooling jacket. Strategically placed thermocouples allowed the temperatures inside the cold box to be recorded.

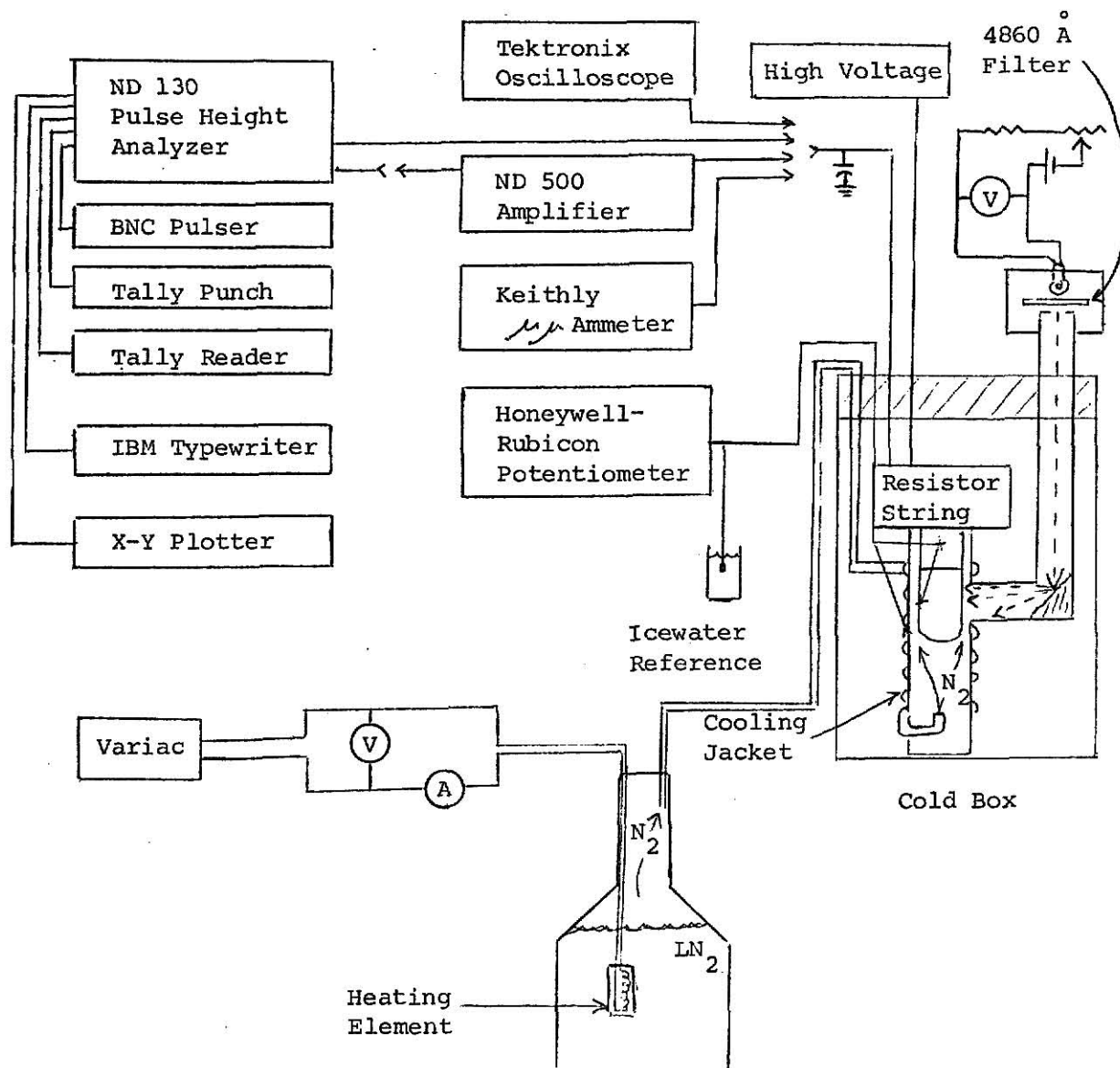


Fig. 5, The Experimental Arrangement

Pulses from the tube were displayed before or after amplification by an ND-500 amplifier on a Tektronix 545 oscilloscope; amplified pulses could also be fed into the ND-130 pulse height analyzer or unamplified pulses fed directly, bypassing the ND-500 amplifier, into the internal amplifier of the pulse height analyzer. The output of the tube could also be fed into a Keithley model 416 picoammeter to measure the dc component of the output current, as these ammeters had sufficiently long time constants to integrate out most of the noise. Output from the pulse height analyzer could be displayed on an oscilloscope, plotted on an xy plotter, or punched on paper tape with a Tally punch. A BNC pulser was used to roughly relate pulse size to channel number and to verify that the analyzer was approximately linear in function. A Honeywell-Rubicon potentiometer monitored three copper-constantan thermocouples with ice water reference junctions; by this method the temperature in the lighttight box, made of a wide mouth Dewar and Styrofoam, could be accurately monitored. Cooling was accomplished by boiling off liquid nitrogen and passing the cold gas through a copper cooling jacket and then over the tube; a coldfinger arrangement was also built in, but never used. A 1.5 V light bulb operated at $\sim .35$ to $.5$ V provided the weak light source.

The light then passed through an interference filter with band width centered at 4860 \AA . The green light emerging from the filter then passed down a plastic pipe to bounce off a rough aluminum surface into the window of the cooling jacket and the photomultiplier. Several tubes were examined before one was finally selected for measurements. The other tubes were rejected because of erratic dark noise, low gain, or both. The tube selected for measurements was an R-106 photomultiplier by Hamamatsu, basically a 1P28 with a quartz window. The R-106 is a tube with an S-19 cathode response (Cs Sb), nine stages of multiplication, and a tube gain of the order of 10^6 . The S-19

cathode response was considered to be useful in other work now going on because of the high quantum efficiency ($\sim 20\%$) towards the blue end of the spectrum, so this type of tube was of some practical interest.

The tube itself is a compact, electrostatically focused side window tube. Due to the electrostatic focusing properties of the tube, it was found that altering the cathode-first dynode voltage produced a radical change in the pulse height distribution. The pulse height distribution for approximately double the cathode-first dynode potential looked very much like those obtained by connecting the cathode to or back-biasing from the first dynode. Unfortunately, for the same overall tube voltage, the tube suddenly experienced a drastic increase in dark current and no further data was taken, in order not to risk damaging the tube. This effect fits the experience of Bertolaccini and Cova (1963); some of their photomultiplier tubes underwent sudden spontaneous increases in dark current on cooling, preceded by large increases in tube gain. Other tubes tested before this report also exhibited large discontinuous dark current changes upon increase of tube voltage or light signal or merely for no apparent reason. The R-106 experienced highly variable dark current, ultimately swinging over to a self-sustaining large dark current upon increase of tube voltage above about 1150 volts.

The green filter was chosen primarily to cut down light intensity from the bulb; at $\sim .4$ V on the bulb it just barely glowed orange, and through the green filter it was virtually invisible. A blue filter would have been better, but green was easily available. The color of the incident light was not considered important, as an experiment performed with a 1P28 tube, of S-5 response, had no detectable difference in the normalized pulse height spectra due to light for the Na yellow line at 5896 \AA vs the Na blue line at 4668 \AA . The glass of the filter also stops much infrared which can change the cathode

temperature by as much as 40° C.

The temperature response in dynode gain and quantum efficiency of the 1P21 type tube is very important, but, since it is recognized as existing, varies greatly from tube to tube, and the R-106 was to be run at -76° C, no attempt was made to investigate these effects. The temperature for the data obtained is noted along with the data.

Data were obtained with only weak illumination of the photocathode. In every instance save one the live time of the analyzer did not go below about 90% and illumination of the photocathode never lowered the live time less than 5%. This high live time eliminated pulse pile up effects. At low temperatures a tendency of the dark noise to be greater after illumination than before was noted; the effect, if present, was masked at room temperature by the magnitude and variability of the dark current. Alternately illuminating the cathode and then counting for one minute periods over a ten minute interval produced a slight apparent change in the dark pulse height distribution; the effect was small, however, for any one minute period, and was probably due to the comparatively bright light warming the cathode slightly. In photon counting with the light intensity so low that the minute dark noise of the R-106 at low temperatures is a detriment to detecting the light signal, no appreciable warming of the cathode is to be expected. Consequently, when long period counting times were used to obtain more reasonable signal-to-noise ratios, no attempt was made to illuminate the tube intermittently during the count. Illumination from the flashlight bulb tended to vary somewhat over a minute's time until a larger battery and higher filament temperature, made possible by a pin hole aperture, improved stability. If live time and anode current may be believed, the bulb would change its illumination by 100% over short time intervals when operated at very low currents.

The high voltage tended to drift by about 10 volts immediately after a new voltage was set on the power supply. Indicated voltage was correct and any fluctuations in high voltage were quite slow, certainly of no importance over the counting times used.

The temperature in the cold box was practically instantaneously reported by the thermocouples; the temperature in the tube was allowed to come to equilibrium over the space of one to four hours, depending on the magnitude of the temperature change. The best indicator of the internal conditions of the tube was the dark current. Down to about -50°C the dark current offered a fairly reliable gauge as to whether the tube was or was not in equilibrium.

In addition to temperature, prior illumination was also a factor in dark current. Above about 1150 V the dark current was apt to spontaneously increase so much that it drove the analyzer to zero live time upon moderately strong illumination of the photocathode. The analyzer would go from 100% live time with a dark tube to 80% live time with the tube illuminated. The live time would then drop rapidly to zero, even without further illumination of the photocathode. With a warm tube proportionately less light was required for this to occur. With a 1P21 tube at high voltage this condition persisted with no light with no apparent diminution for half an hour. Dark current was still very unstable unless the tube had "rested" for a day or more. This effect was apparently difficult if not impossible to induce at lower voltages. The effect may be due to ionization of remaining gas in the envelope as light alone without high voltage had no such effect on the tube. High voltages were avoided after the R-106 exhibited this behavior.

The shape of the dark current distribution apparently did not change after such a period of high dark current; even if the level of dark current was not the same for the same indicated temperature on different days, the

proportions of the distributions are the relevant parameters.

Data taken were stored on paper tape in about two minutes and further measurements made to avoid the risk of temperature or voltage change in the interim. The paper tape was printed or plotted out at leisure and the results processed.

DATA REDUCTION

Data were taken in paired sets: with the light on and off. Current readings were taken with and without illumination; the total number of single photoelectron responses after dark noise subtraction then yielded the average interstage gain. Data were obtained at temperatures ranging from near room temperature to below that of dry ice.

Results were key punched from the analyzer printout and put into a program that corrected for dark counts, normalized, found totals above and below a given channel, converted channel number to fractions of the mean pulse height, found the relative variance, and found the total number of pulses. This program is presented in the Appendix. The program was quite inexpensive to run.

Prescott's iteration formulae for pulse height distributions were programmed for the IBM 360/50 computer; this program was quite expensive to run. The program is included in the Appendix. It may be noted in Plates III and IV how rapidly the distribution assumes its final shape. Note that it is very nearly linear on a semi-log plot as it falls to zero.

A rough estimate of the value of b was obtained from the graphs presented by Prescott. The value of μ was found to be about 5-6 and by inspection of Prescott's results one can see that $b \sim 0.2$. A better value of b was found by comparing the relative variance computed for various values of μ and b to that found experimentally.

It was assumed that the best signal-to-noise ratio would be obtained by rejecting all pulses above or below the value for which a dark pulse height distribution would have greater fractional population than a light distribution of equal number of pulses. Consequently, the total counts above and below a given channel were computed for both light and dark counts for each

of the pulse height distributions analyzed.

Several values of μ were obtained for various voltages and temperatures and are presented in Table I. Pulse height distributions both with and without light for various values of high voltage and temperature are presented in Plates V - XI and XX - XXIX. Discriminator levels for the varying tube voltages and temperatures were chosen. The upper and lower discriminator levels chosen were selected by use of the signal-to-noise plots, Plates XV - XIX, and tables in which the light and dark counts between two given channel numbers were divided to obtain signal-to-noise ratios, Tables VI - X. In view of the fact that signal-to-noise ratios were computed on the basis of the signal counting rate being equal to the dark counting rate, dark count rates observed for a variety of voltages and temperatures are presented in Table IV. Computed values for the relative variance for different values of μ and b , Table II, were compared to the relative variances obtained experimentally and shown in Table III. Due to the high gain, corrections for the number of cascades that broke were insignificant, as demonstrated by Table IV. Due to the presence of the high amplitude tail in the single electron pulse height distribution the data were truncated at various levels and the variances computed for the abbreviated distributions as well as the complete distributions.

In an effort to determine the single electron response the photocathode was back-biased in varying degrees; this apparently defocused the electron multiplier structure as demonstrated by Plates XII - XIV. In an attempt to enhance the single electron response the cathode-first dynode voltage was approximately doubled; this defocused the structure, but before good data on this phenomenon could be obtained the dark noise increased spontaneously and the measurement was discontinued.

TABLE I

Gains and Mean Inter-stage Gains

Obtained at Various Operating Voltages and Temperatures

Run No.	Temperature Degrees C	Tube Voltage	Gain $\times 10^6 \pm \%$	Mean Inter- Stage Gain
146**	-83 ± 5	1150	5.0 ± 10	5.5
133B*	-77 ± 5	1150	2.2 ± 30	5.0
179***	-77 ± 5	1105	9.1 ± 13	5.9
181***	-102 ± 5	1100	8.3 ± 25	5.9
143**	-83 ± 5	1100	4.8	5.5
145**	-83 ± 5	1100	3.8 ± 33	5.4
147**	-83 ± 5	1100	4.0 ± 20	5.4
124*	-65 ± 5	1100	2.0 ± 30	5.0
162+	-54 ± 5	1100	13.6 ± 27	6.2
142**	-18 ± 3	1100	4.8 ± 40	5.5
157++	$+21 \pm 5$	1100	2.0 ± 100	5.0
165***	$+21 \pm 5$	1100	4.3 ± 110	5.5
175***	-77 ± 5	1005	2.5 ± 80	5.2
149**	-83 ± 5	1000	1.8 ± 50	4.9
170***	$+22 \pm 5$	1000	0.36 ± 20	4.1
150**	-83 ± 5	950	1.4 ± 170	4.8
151**	-83 ± 5	900	$4.3 \pm$	5.5
174**	-73 ± 5	900	0.95 ± 20	4.6

* Data Taken 18 May 1970.

** Data Taken 3 June 1970.

*** Data Taken 20 June 1970.

+ Data Taken 19 June 1970.

++ On exposure to light on the next run the tube noise spontaneously increased.
Data Taken 19 June 1970.

TABLE II

Relative Variances Based on Prescott's Theory (1966)

Mean Interstage Gain $\mu = 5$

b	0	.1	.2	.3	.4	.5	.6	.7	.8	.9	1.0
V	.25	.375	.50	.625	.75	.875	1.0	1.125	1.25	1.375	1.5

Mean Inter-stage Gain $\mu = 6$

b	0	.1	.2	.3	.4	.5	.6	.7	.8	.9	1.0
V	.20	.32	.44	.56	.68	.80	.92	1.04	1.16	1.28	1.4

TABLE III

Run	Voltage (Volts)	Temperature (Degrees C)	Mean Factor*	Truncation Pt.		Rel. Var.	f(x)
				Ch. No.	P. Ht.		
181	1100	-102 ± 5	0.82	260	4.37	0.29	0.972
			0.87	300	5.04	0.48	0.980
			0.91	350	5.87	0.71	0.987
			0.94	400	6.72	0.89	0.992
			0.97	450	7.56	1.04	0.995
			1.0	511	8.58	1.24	1.0
179	1105	-77 ± 5	0.80	200	3.55	0.017	.962
			0.85	250	4.41	0.31	0.975
			0.89	300	5.30	0.54	0.984
			0.92	350	6.18	0.71	0.989
			0.95	400	7.06	0.85	0.993
			1.0	511	9.02	1.18	1.0
147	1100	-83 ± 5	1.0	511		0.83	1.0
			0.85	Less Exponential		0.33	1.0
124	1100	-65 ± 5	1.0	511		0.46	1.0
176	1005	-77 ± 5	0.84	200	8.71	0.19	0.979
			0.89	250	10.89	0.52	0.989
			0.93	300	13.07	0.81	0.994
			0.96	350	15.25	1.19	0.998
			0.99	400	17.43	1.58	1.000
			1.0	511	22.26	1.70	1.0
170	1000	$+22 \pm 5$	1.0	511		0.70	1.0
174	900	-73 ± 5	1.0	511		1.22	1.0
			---	Less Exponential		0.51	1.0

* The Mean Factor is the number that the old mean must be multiplies by in order to obtain the value of the mean for the truncated data.

TABLE IV

Fraction k of Cascades That Fail to Propagate

Data Taken from Prescott (1966)

Polya Shaping Parameter, b	Mean Stage Gain, μ					
	3.0	3.5	4.0	4.5	5.0	6.0
0.0	0.060	0.034	0.020	0.012	0.007	0.003
0.1	-----	0.058	0.039	0.026	0.018	0.009
0.2	0.12	0.084	0.060*	0.045	0.034	0.020
0.3	-----	0.11	0.084	0.066	0.052	-----
0.4	0.18	-----	0.11	-----	-----	-----
0.5	0.21	-----	0.13	-----	-----	-----
0.6	0.24	-----	-----	-----	-----	-----
0.8	0.29	-----	-----	-----	-----	-----
1.0	0.33	-----	-----	-----	-----	-----

* Interpolated by Prescott.

An additional value is $\mu = 2.0$, $b = 0.5$, $k = 0.38$.

TABLE V

Typical Dark Count Rates for The R-106

Run	Temperature *C	Voltage V	Counts/Minute
178	-77 \pm 5	1105	29.5
144	-78 \pm 5	1110	48.8
124B	-65 \pm 5	1100	23,300*
147A	-83 \pm 5	1100	59
180	-102 \pm 5	1100	20.0
148A	-82 \pm 5	1050	66
175	-77 \pm 5	1005	23.3
169	+22 \pm 5	1000	11,966
141B	-10 \pm 2	1000	676
149A	-83 \pm 5	1000	39
150A	-83 \pm 5	950	29
141C	-10 \pm 2	900	21.9
174	-73 \pm 5	900	68.5
151B**	-83 \pm 5	900	30
151C**	-83 \pm 5	900	12.9

* Tube probably not yet in electronic equilibrium.

** Run 151B was a 1 minute count after exposure to light;
151C was a 10 minute count thereafter. Temperature and voltage did
not change.

TABLE VI

Percent Improvement in Signal-to-Noise Ratio by Use of

Upper and Lower Discriminator Levels. Run 174A-B, 900 V, $-73 \pm 5^\circ \text{C}$

Upper Level Chl. No.	30	40	50	80	511	% Signal Lost
Lower Level Chl. No.						
0	0.2	0.3	0.3	0.3	0	0
5	4.2	4.3	4.3	4.3	3.6	45
10	8.4	8.5	8.3	8.2	6.5	77
15	14.6	15.8	13.4	12.7	8.3	91

TABLE VII

Percent Improvement in Signal-to-Noise Ratio by Use of

Upper and Lower Discriminator Levels. Runs 169-170, 1000 V, $+22 \pm 5^\circ \text{C}$

Upper Level Chl. No.	40	45	60	511	% Signal Lost
Lower Level Chl. No.					
0	4.4	4.3	3.3	0	5
5	23.6	23.0	20.8	15.4	12
10	40.8	39.3	35.1	26.5	32
15	50.9	48.0	41.2	28.4	50

TABLE VIII

Percent Improvement in Signal-to-Noise Ratio by Use of

Upper and Lower Discriminator Levels. Runs 175-176, 1005 V, $-77 \pm 5^\circ \text{C}$

Upper Level Chl. No.	30	40	50	70	90	511	% Signal Lost
Lower Level Chl. No.							
5	13.2	----	9.5	8.8	7.5	4.5	10
7	17.1	13.7	12.1	11.4	---	---	29
10	14.6	----	9.5	8.6	7.0	3.4	38

TABLE IX

Percent Improvement in Signal-to-Noise Ratio by Use of

Upper and Lower Discriminator Levels. Runs 178-179, 1105 V, $-77 \pm 5^\circ \text{C}$

Upper Level Chl. No.	60	70	75	80	85	90	511	% Signal Lost
Lower Level Chl. No.								
11	25.3	26.2	24.4	22.9	22.1	22.1	14.0	24
12	25.7	30.9	24.8	23.2	22.4	22.4	14.9	25
13	25.6	26.6	24.8	23.1	22.3	22.3	16.5	28

TABLE X

Percent Improvement in Signal-to-Noise Ratio by Use of

Upper and Lower Discriminator Levels. Runs 180-181, 1100 V, $-102 \pm 5^\circ \text{C}$

Upper Level Chl. No.	55	60	65	70	75	80	% Signal Lost
Lower Level Chl. No.							
5	6.3	11.1	6.4	5.9	4.9	5.5	29
10	12.7	12.4	12.0	---	6.6	7.5	34
15	17.8	16.9	16.2	---	13.5	13.9	38
20	22.2	20.8	19.7	---	16.2	16.6	44
25	21.7	20.2	19.0	---	15.2	15.7	51

RESULTS AND CONCLUSIONS

Examination of single electron pulse height spectra with Prescott's curves superimposed indicated that $\mu = 5$ or 6 and $b \sim .2$. The correspondence was not exact, the principal difference being that the experimental data had a high amplitude tail extending from about two and one half mean pulse heights to nine or more mean pulse heights. The relative variances computed from the extended data would indicate a b value close to unity, which from the shape of the spectra was considered impossible. The data were then truncated and a relative variance computed for each truncation. At about four and one half mean pulse heights the variance became close to that to be expected from $\mu = 5$ or 6 and $b \sim .1$, as may be seen in Table III. Further truncation would further reduce the variance so that b could equal zero on this basis; inspection of the graph indicates this value to be unlikely.

The high amplitude pulses were found to be dependent on the total number of pulses counted, but the dependence was not linear. For run 179, performed at 1105 volts and -77°C , the total number of pulses beyond channel 300, or about five mean pulse heights, were counted. The light distribution had 8.6 times as many pulses beyond channel 300 as the dark pulse distribution; the light pulse height distribution had 13.9 times as many pulses in all and the dark pulse distribution had an integration time 40 times as long as the light pulse distribution. It is interesting to note that when the pulse height distribution for a back-biased photocathode was subtracted from the normal dark pulse distribution the high amplitude tail remained. This implies that the tail is due to the photocathode. This fits well the hypothesis that cosmic ray or natural fluorescence in the glass or cathode material causes high amplitude pulses. If there were a time dependent noise mechanism, such as

radiation, and a population dependent mechanism such as residual gas fluorescence or just a very high gain section of dynode, this would require that 11 out of 30 high amplitude noise pulses be due to time dependent processes. This would mean a noise counting rate of about one high amplitude pulse every four minutes, a not too unlikely possibility. If one takes the data of Verde, et. al., on high amplitude pulses literally, the pulses under consideration would correspond to an energy range of about two to five KeV. The residue of the high energy pulses would then be proportional to population. A mechanism such as residual gas ionization or a small, exceedingly high gain area of dynode surface would explain this phenomenon.

As mentioned above, in an effort to fit the probability distribution predicted by Prescott, the data were truncated. Much the same effect on b was obtained by subtraction of a long period exponential from the data, though this in turn engendered some lumps in the resulting distribution. In addition, simply truncating the data resulted in a reasonable graphic fit with $b \approx .2$. If Prescott's Polya probability distribution theory is correct, and if one considers any local patch of high gain dynode surface to act independently of the rest of the dynode and be reasonably uniform across its surface, then one is left with a more nearly "triangular" component rather than an exponential. The low amplitude end of the observed distribution would not then be in conflict with theory. Gas ionization might conceivably produce the same result.

It was found that for tube voltages greater than about 900 V the use of upper and lower discriminator levels would yield about a 20-25% increase in signal-to-noise ratio as seen in Tables VI - X. The lower window level was critical; the upper level was less so. The dual criteria of signal-to-noise ratio and statistics must be considered in applying these tables; if the

increase in signal-to-noise is buried in statistical fluctuations one is not much better off than before. Integration time and counting rate are then the determining factors in deciding to use discriminators. Consequently, information on roughly how much light signal would be rejected by window combinations is included. These figures are an average over the range of values for upper window levels for any one lower window level and are only approximate. Better estimates can be obtained from the signal-to-noise ratio graphs if desired. Since the window levels indicated are dependent on the gain and noise level at which the tube is operated on any given day for any given voltage and temperature, windows must be set in terms of the proportions of a light distribution taken that day. Since use of discriminator levels provides comparatively little improvement in signal-to-noise ratio and cooling the tube should, if large light levels are avoided, provide a low and constant dark current, their necessity is unlikely to occur except where very high amplification might raise the noise due to several dynodes above the natural low response level of the recording device.

In conclusion, then, Prescott's Polya statistics provide a reasonably good description of the R-106 up to about two and one half to four mean pulse heights, with high amplitude pulses above that level distorting the distribution. The source of these pulses is not understood. The observed interstage gain is about five and one half and the Polya parameter $b \sim .1 - .2$. Discriminator levels produce an improvement in signal-to-noise ratio at tube voltages above 900 V, but due to the fact that moderate to large amounts of signal are lost and refrigeration produces such small dark noise, discriminators in the pulse counting mode are unlikely to ever be useful unless the signal is amplified so much that the noise contributions from the second and lower dynodes become appreciable.

EXPLANATION OF PLATE V

Graph of dark pulse height distributions for different tube potentials.

R-106, runs 141 A - D.

Fig. 1.

A. 1100 V, 2 minutes live time.

Fig. 2.

B. 1000 V, 2 minutes live time.

C. 900 V, 4 minutes live time.

D. 800 V, 4 minutes live time.

Temperature $-10 \pm 2^{\circ}$ C.

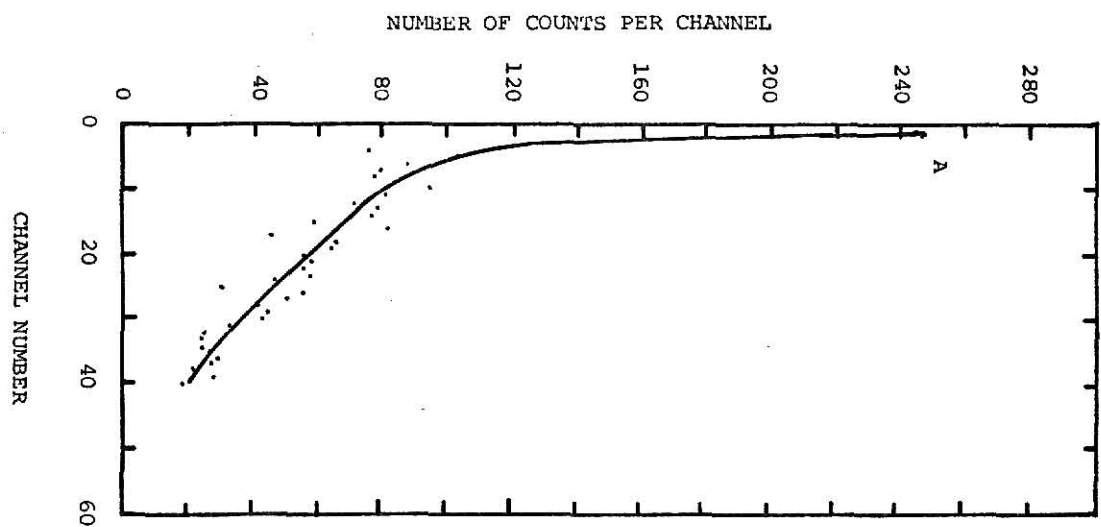


Figure 1.

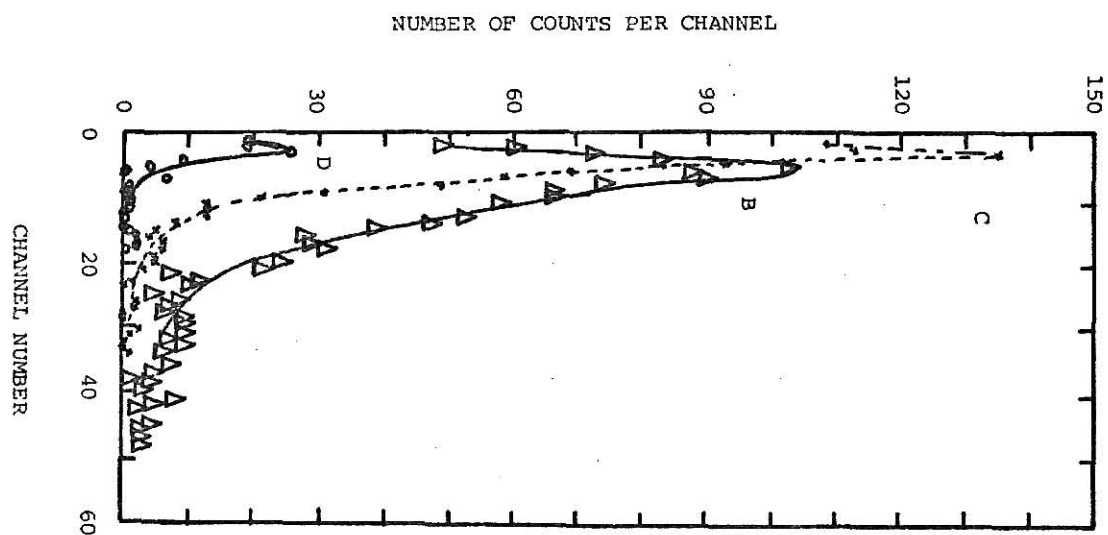


Figure 2.

EXPLANATION OF PLATE VI

Graph of single electron pulse height distribution, 1150 V on photo-multiplier R-106, run 146. Temperature $-83 \pm 5^{\circ}$ C.

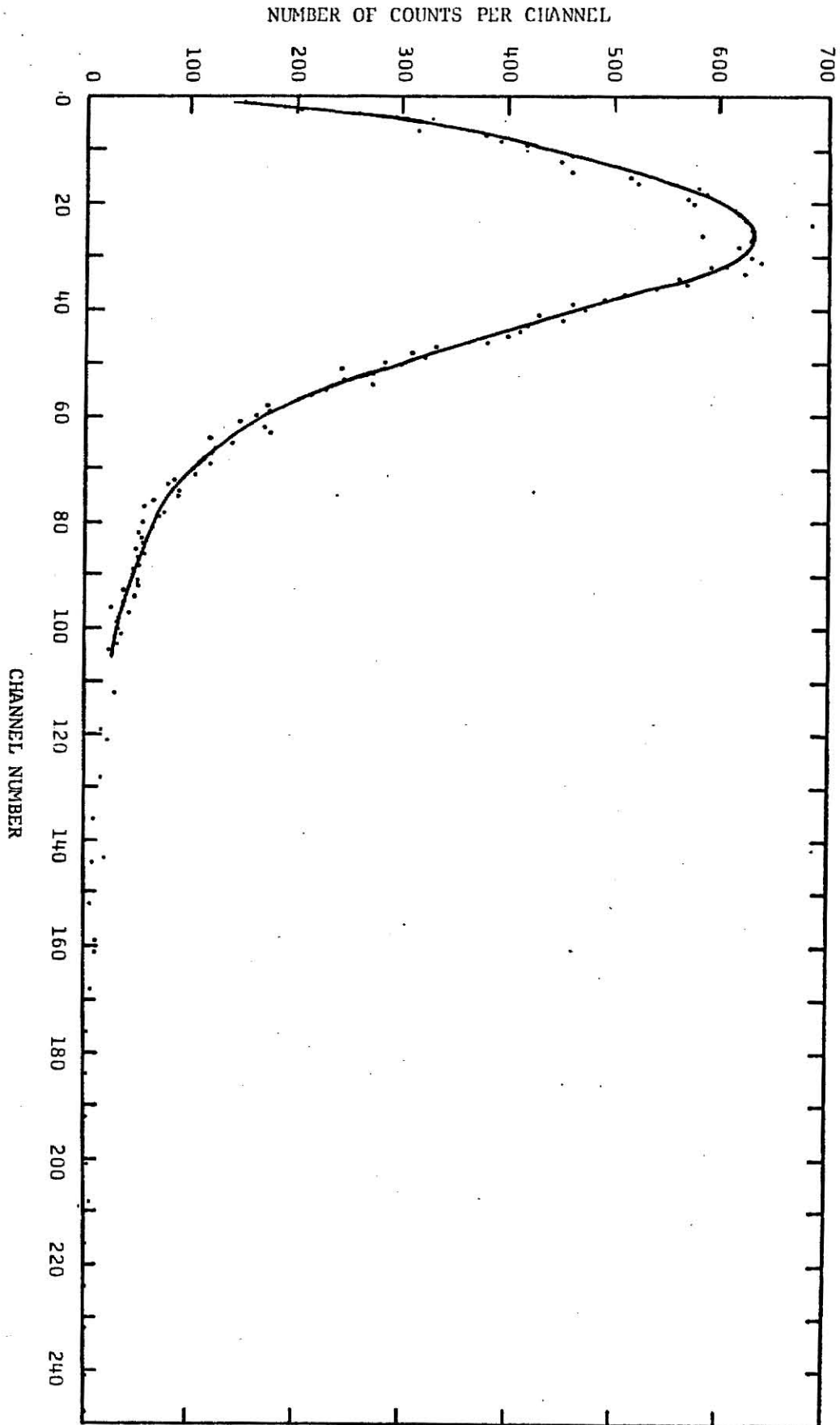
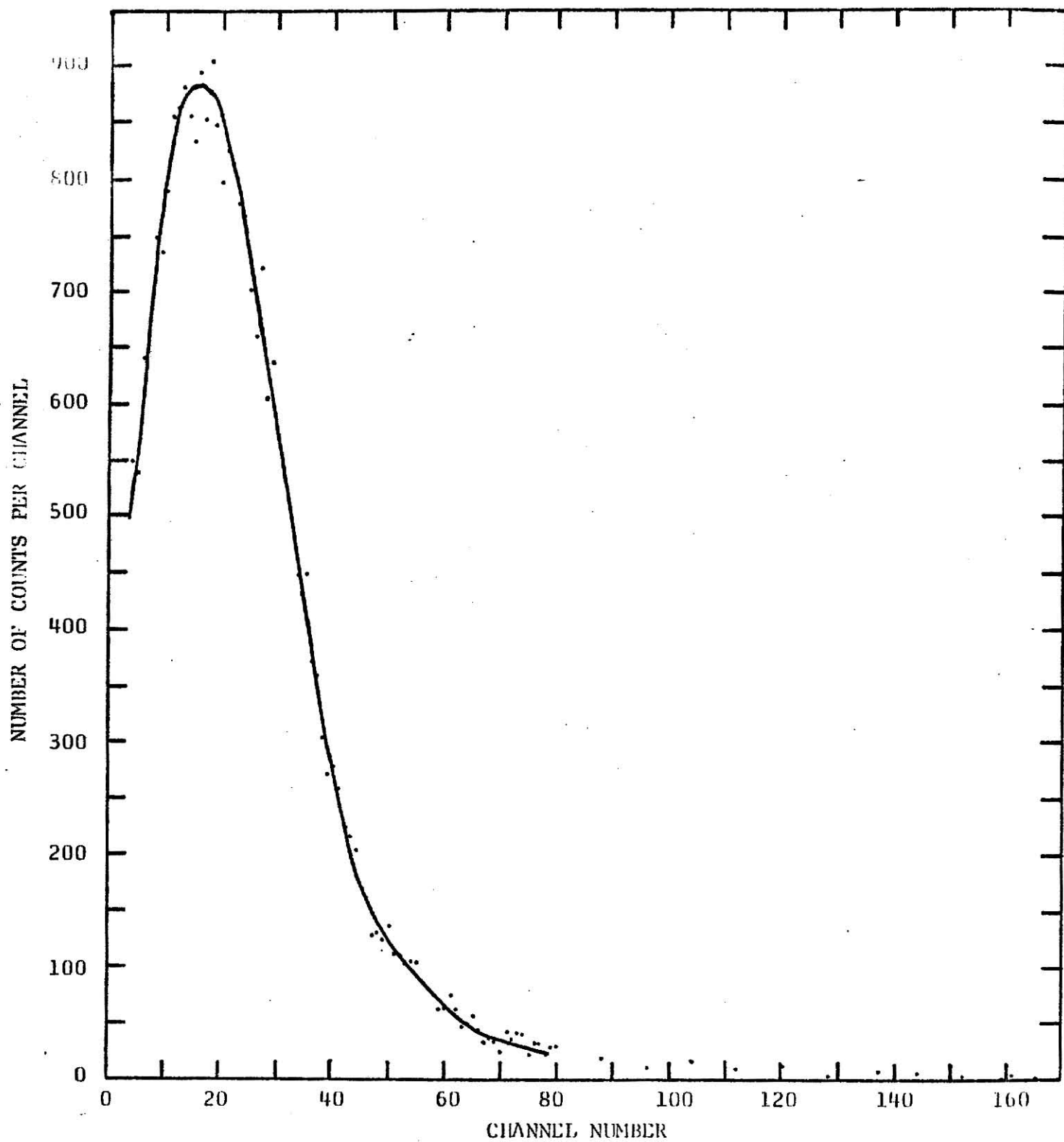


PLATE VI

EXPLANATION OF PLATE VII

Graph of single electron pulse height distribution, 1100 V on photo-multiplier R-106, run 145. Temperature $-83 \pm 5^{\circ}$ C.

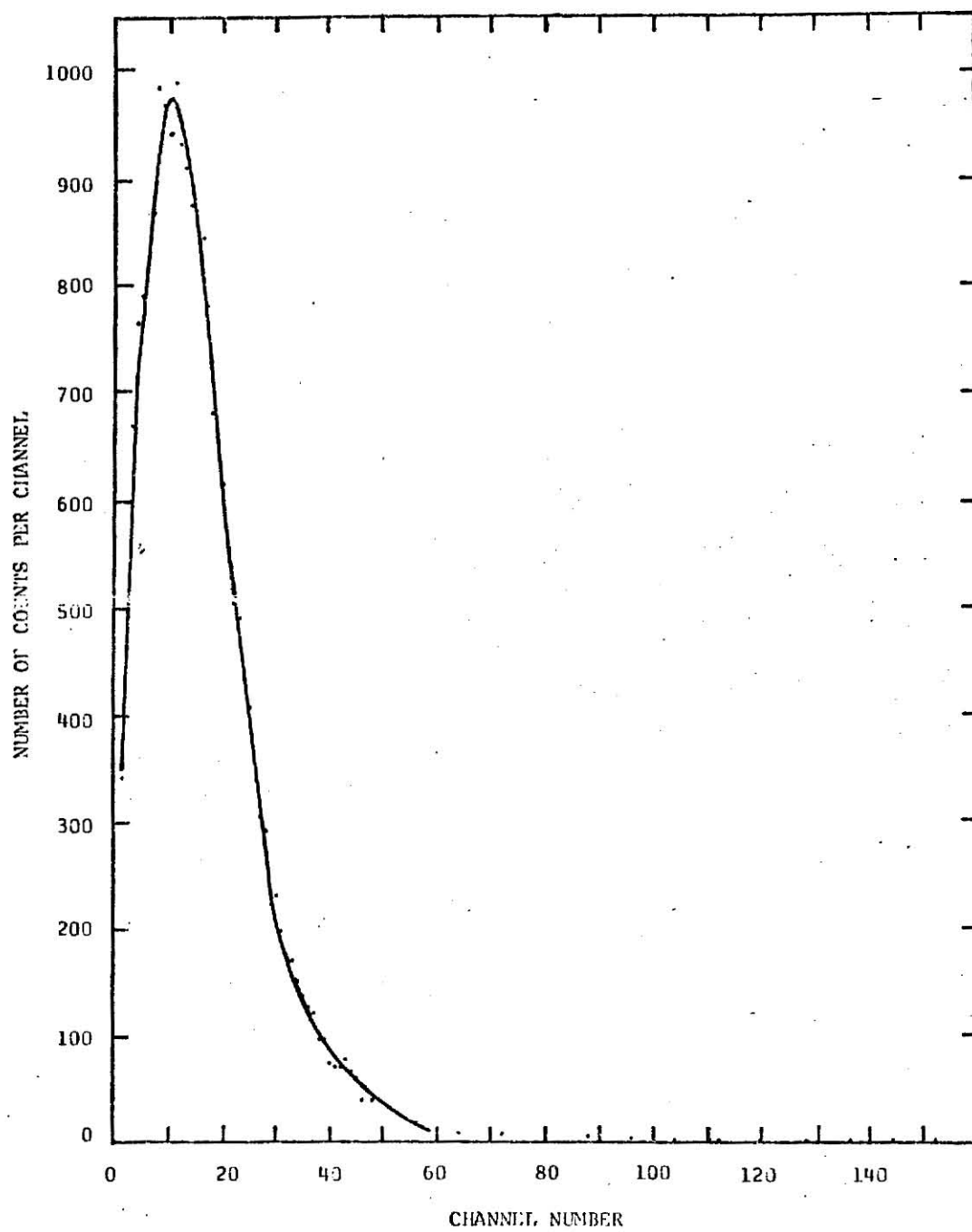
PLATE VII



EXPLANATION OF PLATE VIII

Graph of single electron pulse height distribution, 1050 V on photo-multiplier R-106, run 148. Temperature $-83 \pm 5^{\circ}$ C.

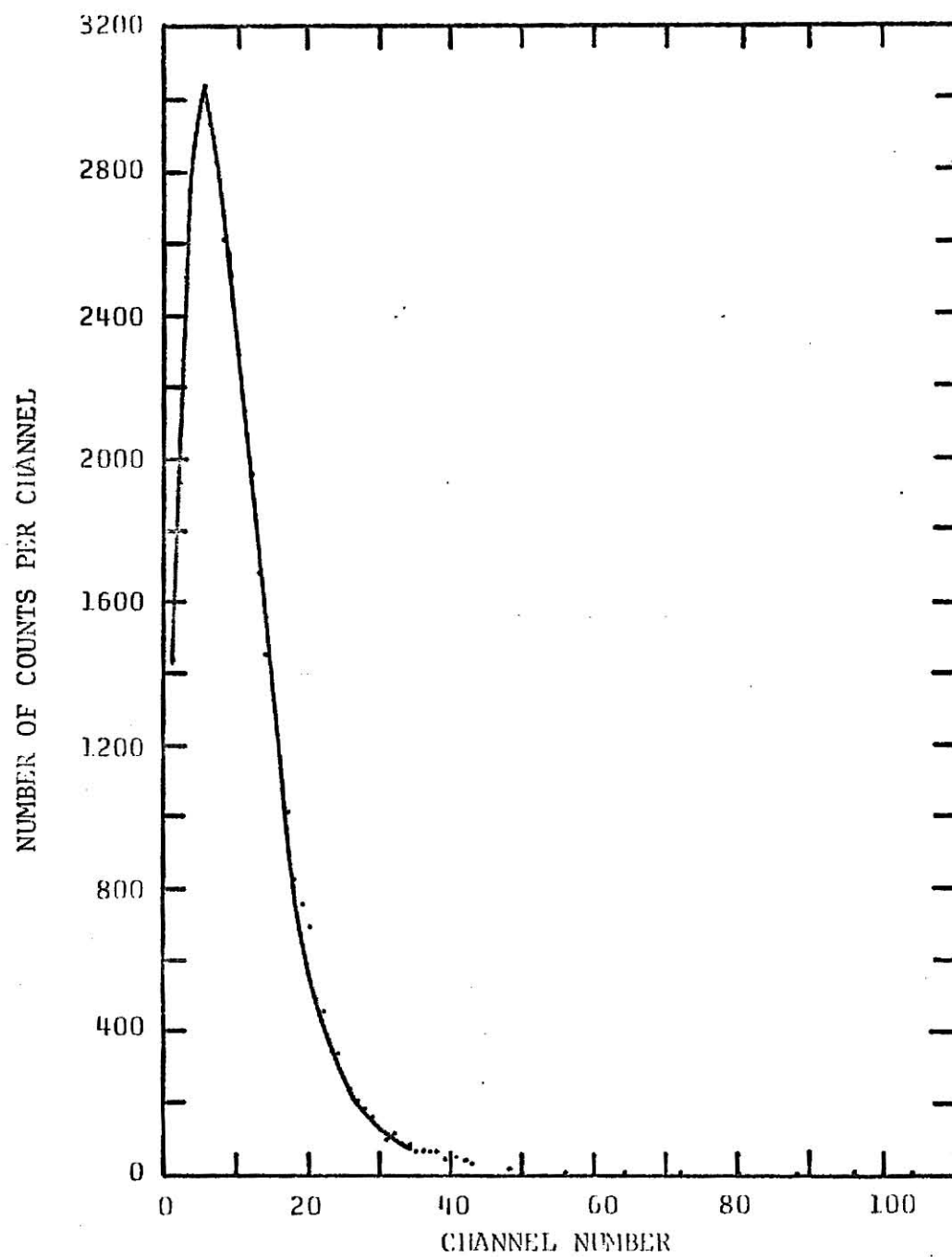
PLATE VIII



EXPLANATION OF PLATE IX

Graph of single electron pulse height distribution, 1000 V on photo-multiplier R-106, run 149. Temperature $-83 \pm 5^{\circ}$ C.

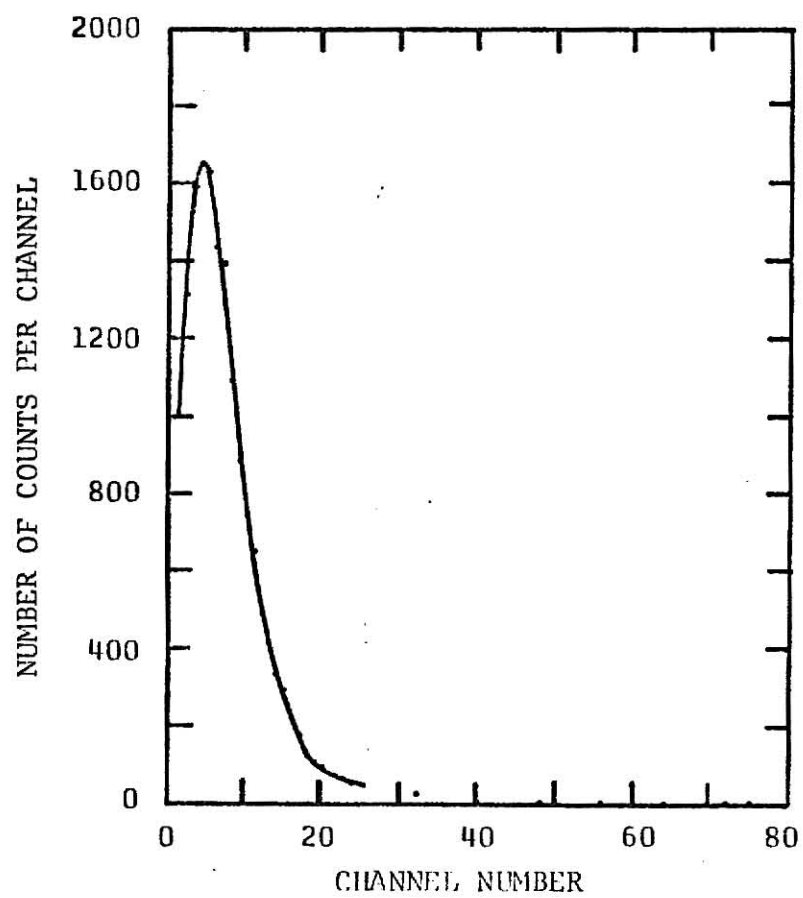
PLATE IX



EXPLANATION OF PLATE X

Graph of single electron pulse height distribution, 950 V on photo-multiplier R-106, run 150. Temperature $-83 \pm 5^{\circ}$ C.

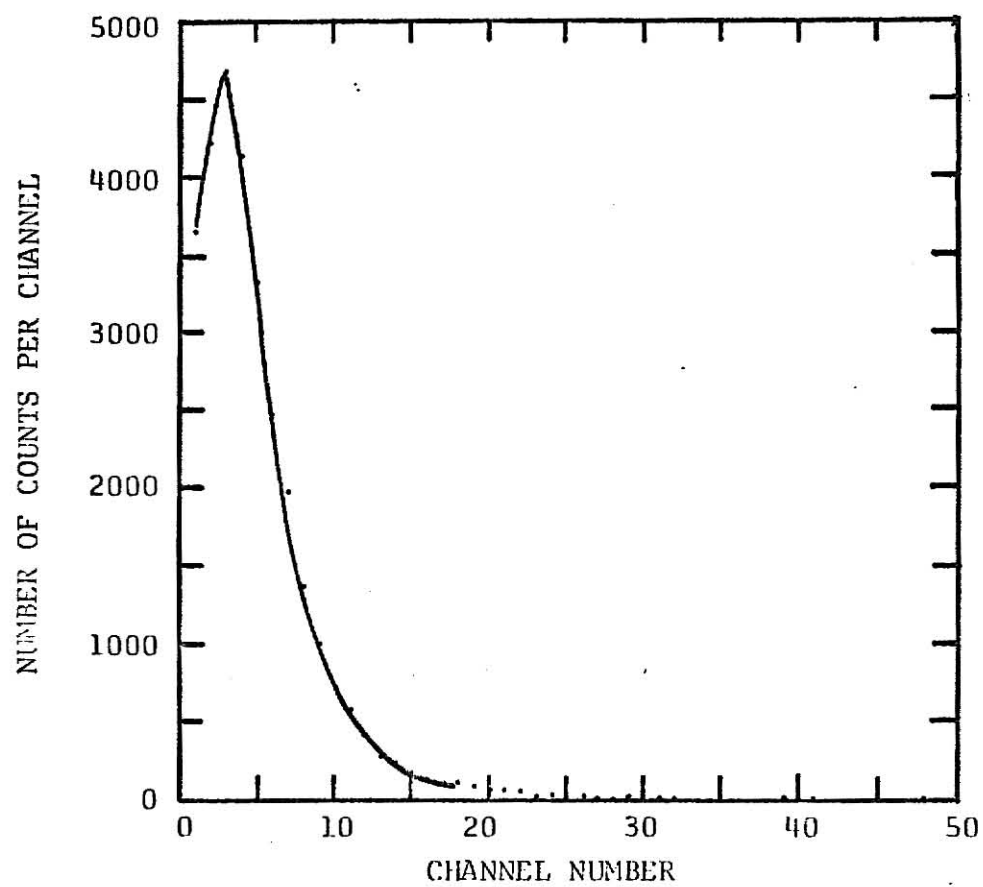
PLATE X



EXPLANATION OF PLATE XI

Graph of single electron pulse height distribution, 900 V on photo-multiplier R-106, run 151. Temperature $-83 \pm 5^{\circ}$ C.

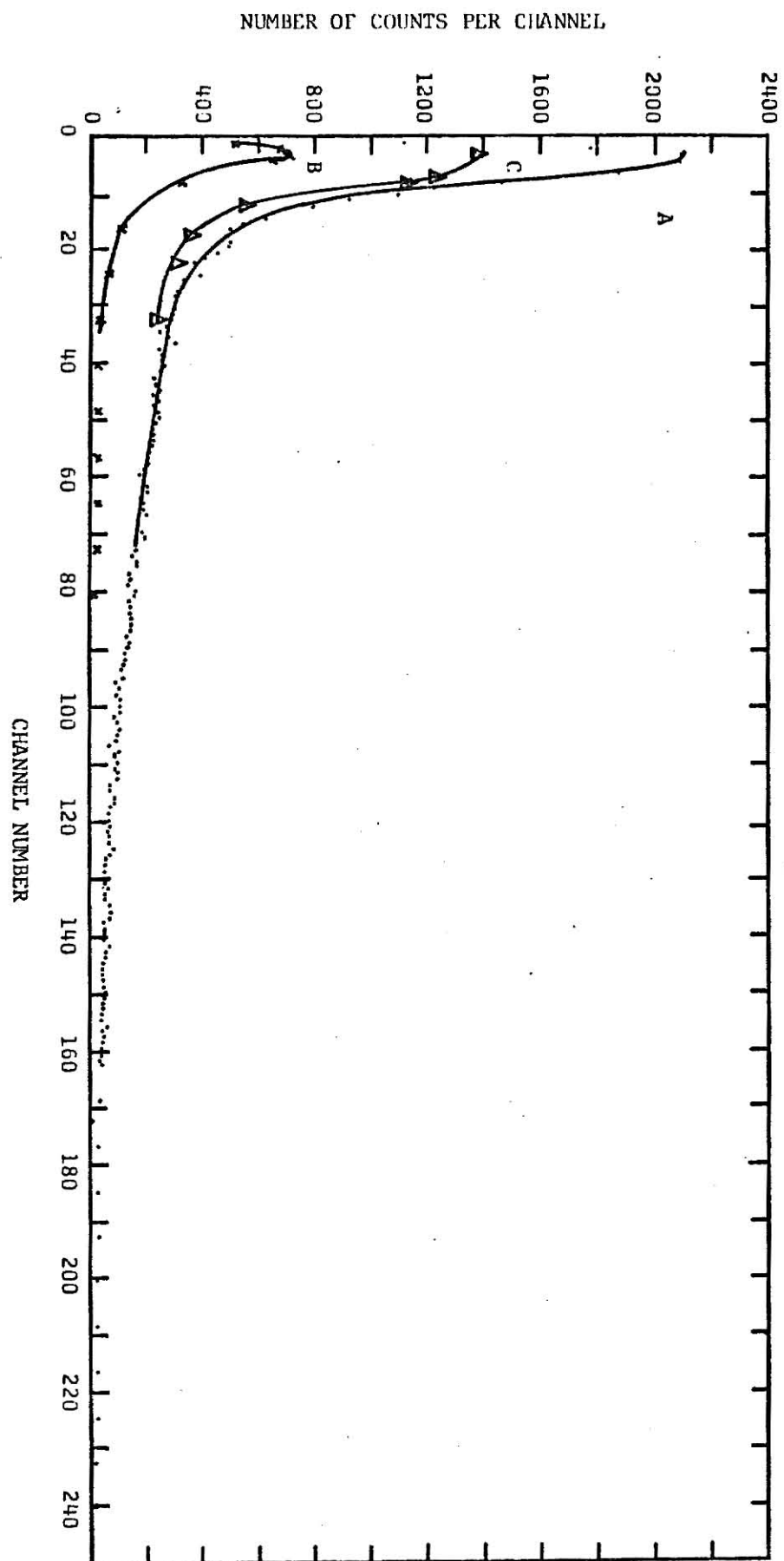
PLATE XI



EXPLANATION OF PLATE XII

Graphs of pulse height distributions obtained from R-106 at $-78 \pm 5^\circ \text{C}$.

- A. Dark noise, photocathode at -125 V with respect to first dynode, run 128.
- B. Dark noise, photocathode at +9 V with respect to first dynode, run 129.
- C. Curve A minus curve B.

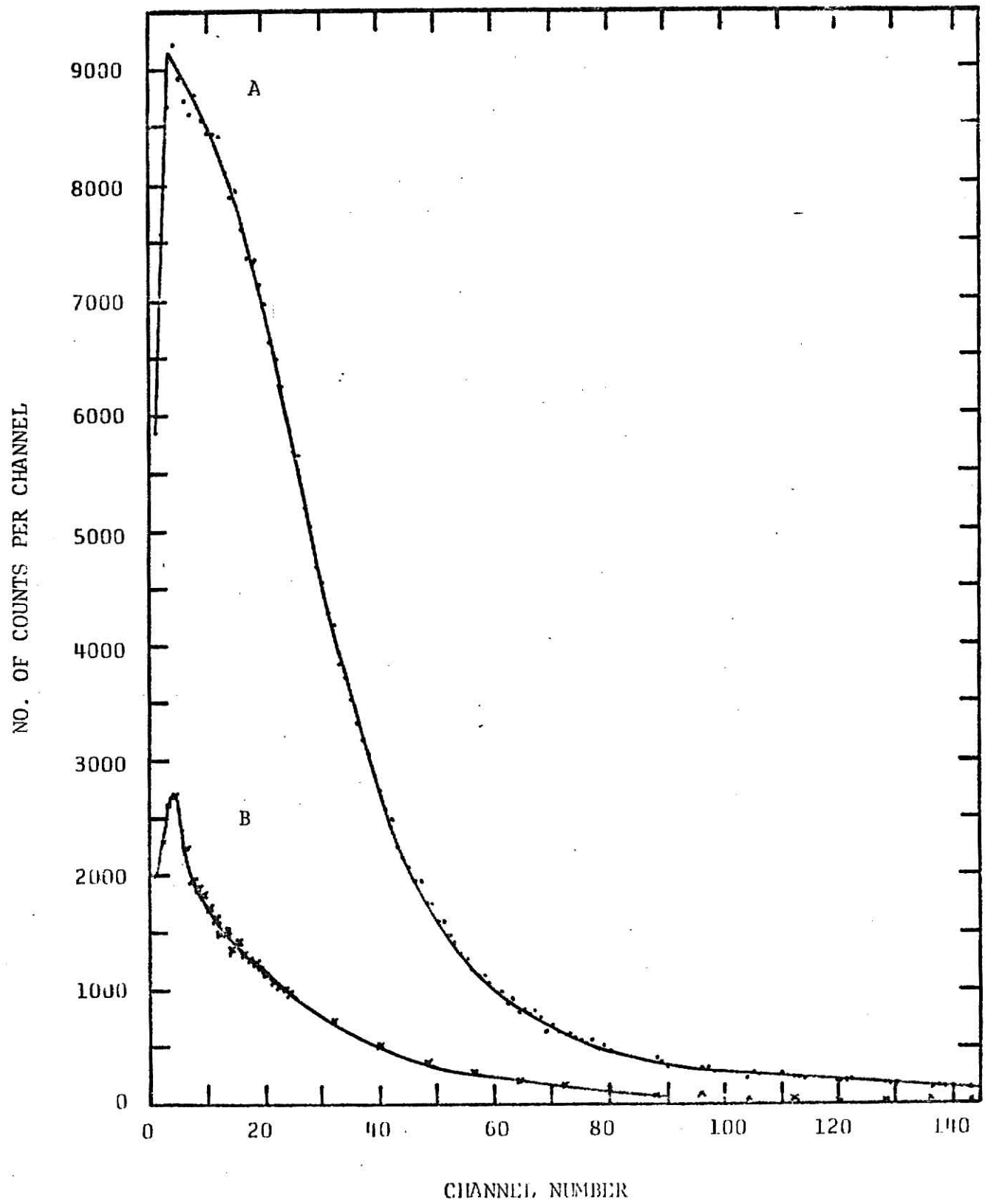


EXPLANATION OF PLATE XIII

Graphs of pulse height distributions due to weak light on R-106 at $-74 \pm 5^\circ \text{ C}$ at 1100 V tube voltage.

- A. Photocathode at -200 V with respect to the first dynode, run 152.
- B. Photocathode at -110 V with respect to the first dynode, run 153.

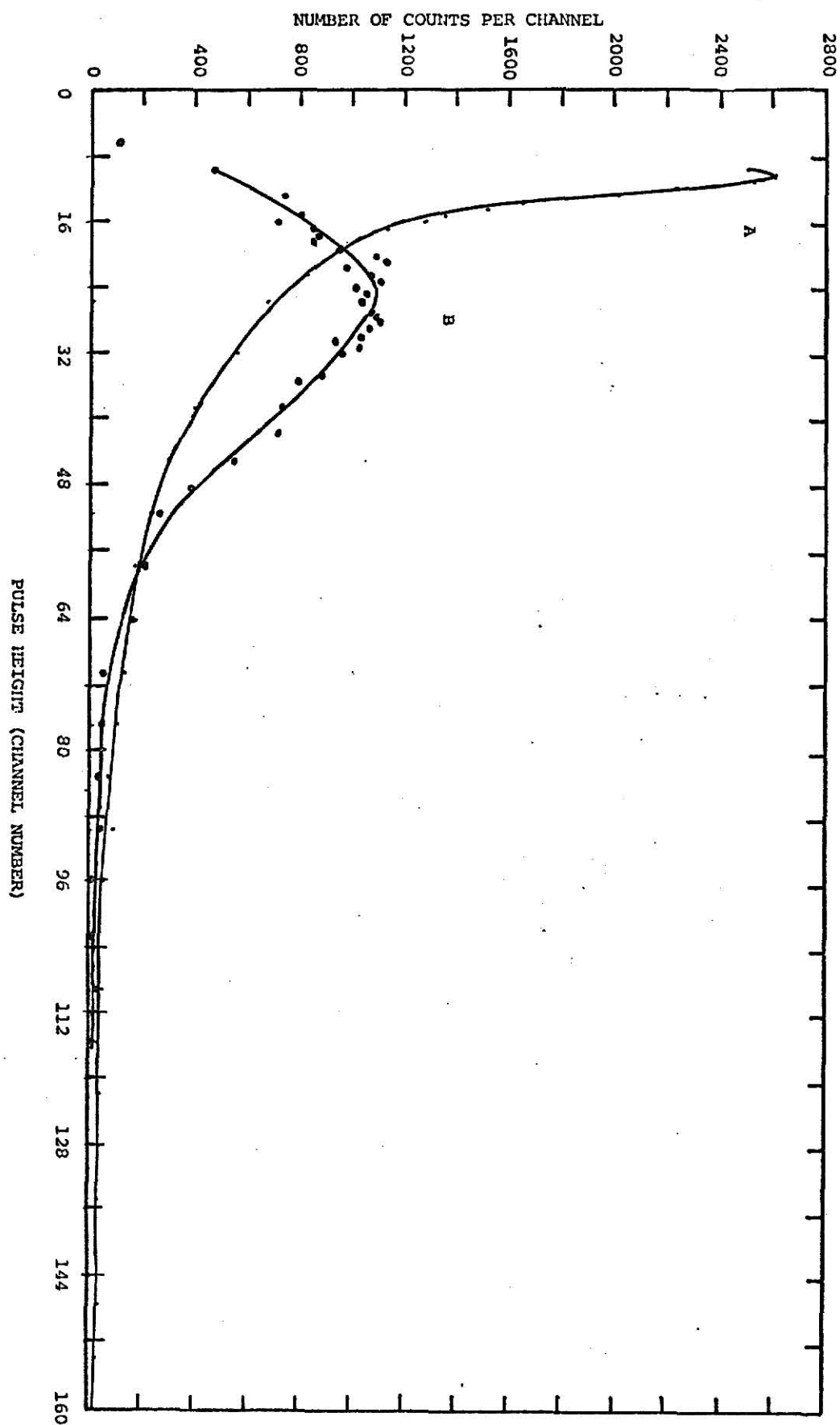
Note the magnitude of the dark noise. Immediately after this measurement the tube degenerated into a very noisy mode of operation, driving the multichannel analyzer to zero percent livetime.



EXPLANATION OF PLATE XIV

Curve A is the single electron response of the R-106 run at 1150 V, -76° C, run 133B. The dark pulse height distribution has been subtracted.

Curve B is the result of run 133A at 1150 V, -76° C, with a standard resistor string with the distribution resulting from back-biasing the photocathode +9 V with respect to the first dynode subtracted.

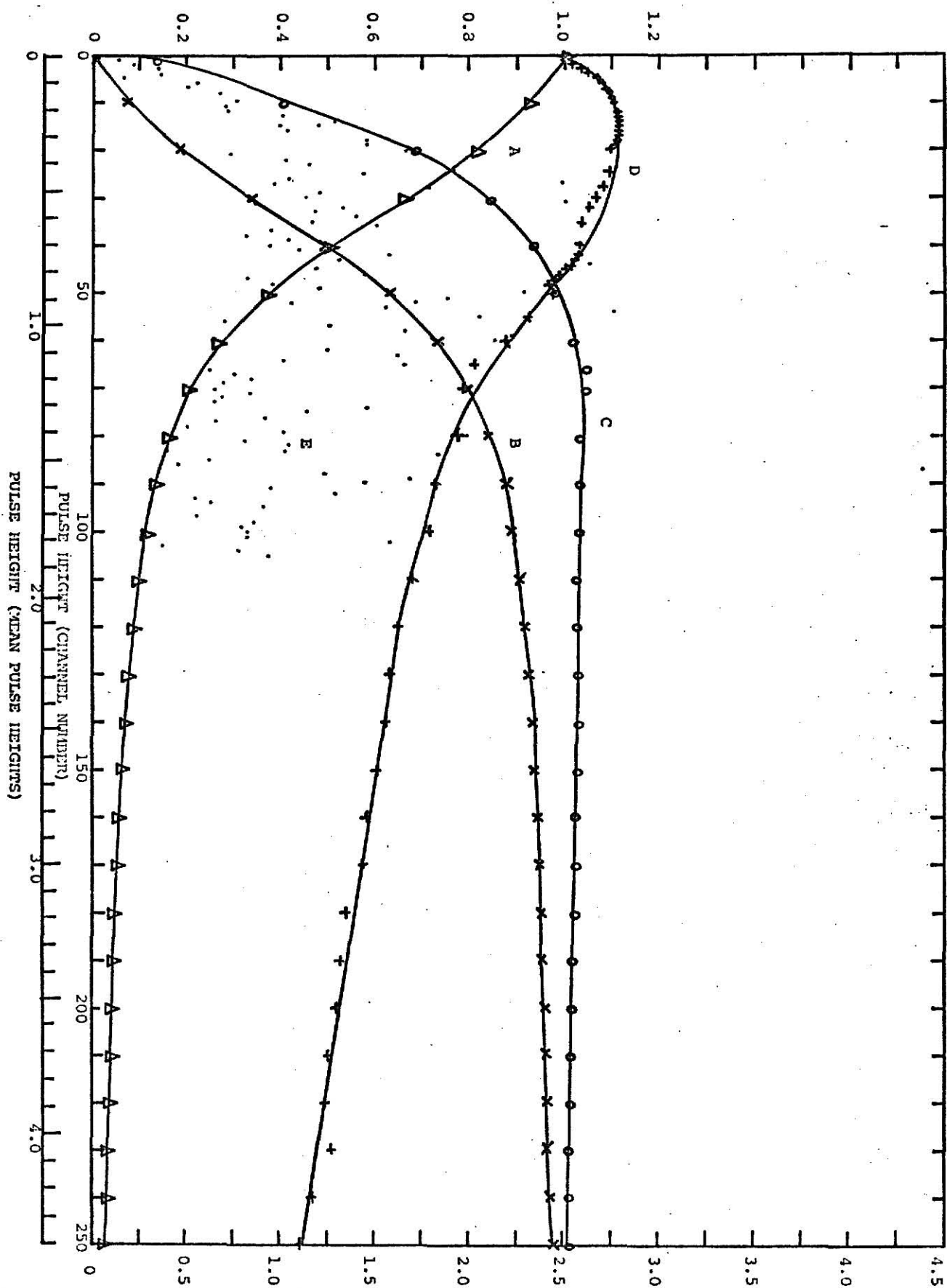


EXPLANATION OF PLATE XV

The graphs are based on the single electron pulse height distribution and noise pulse height distributions for the R-106 run at 1105 V, -77° C, runs 178-179.

- A. Graph A is the total of the normalized population at or above a given channel for the weak light pulse height at or above a given channel for the weak pulse height distribution less the dark pulse height distribution. This is read off the left hand ordinate and is expressed as probability density.
- B. Curve B is the total population of single photoelectron pulses at or below a given pulse size. Like curve A, the left hand ordinate is used.
- C. Curve C is the ratio of the populations of the single photoelectron response at or below a given channel number to the corresponding dark noise pulse height population.
- D. Curve D is the ratio of the single photoelectron response to the dark pulse height distribution at or above a given channel. Both curves C and D use the left hand ordinate and are dimensionless.
- E. Curve E is the ratio of signal to dark pulses in a given channel for populations of equal total numbers of pulses. These are the isolated dots. These are read against the right hand ordinate.

PLATE XV

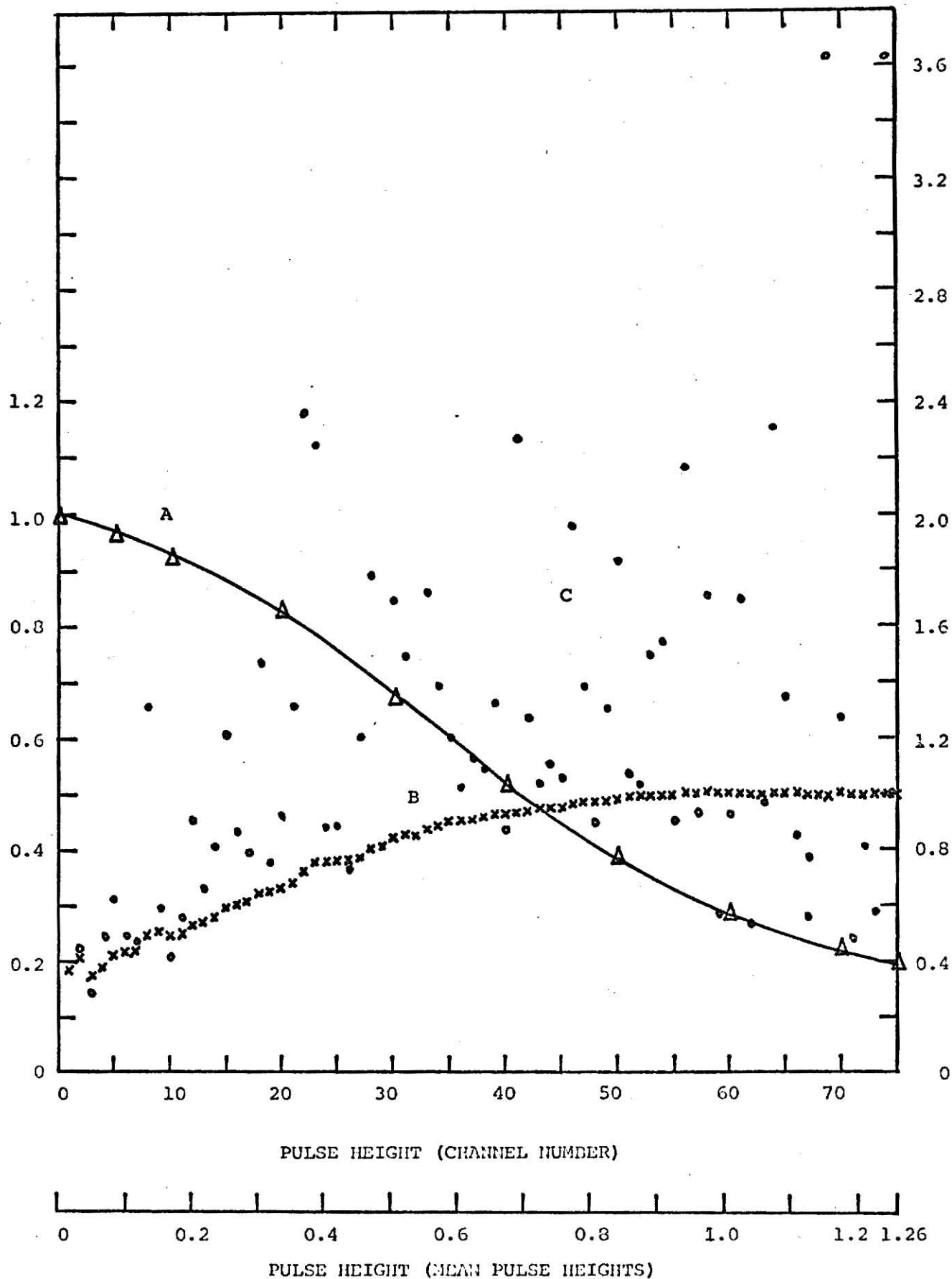


EXPLANATION OF PLATE XVI

Curve A is the normalized population of pulses at or above a given channel number for the single electron response of the R-106 run at 1100 V, -102° C, run 181. The dark pulse height distribution has been subtracted. This graph uses the left hand ordinate.

Curve B is the total amount of signal at or below a given channel divided into the total amount of dark pulses at or below the same channel for runs 180-181. This curve uses the left hand ordinate.

Curve C is the instantaneous signal-to-noise ratio; i.e., the number of counts in a given channel in the light distribution divided by the number of counts in a channel for a dark pulse height distribution of equal total number of counts. This curve uses the right hand ordinate.

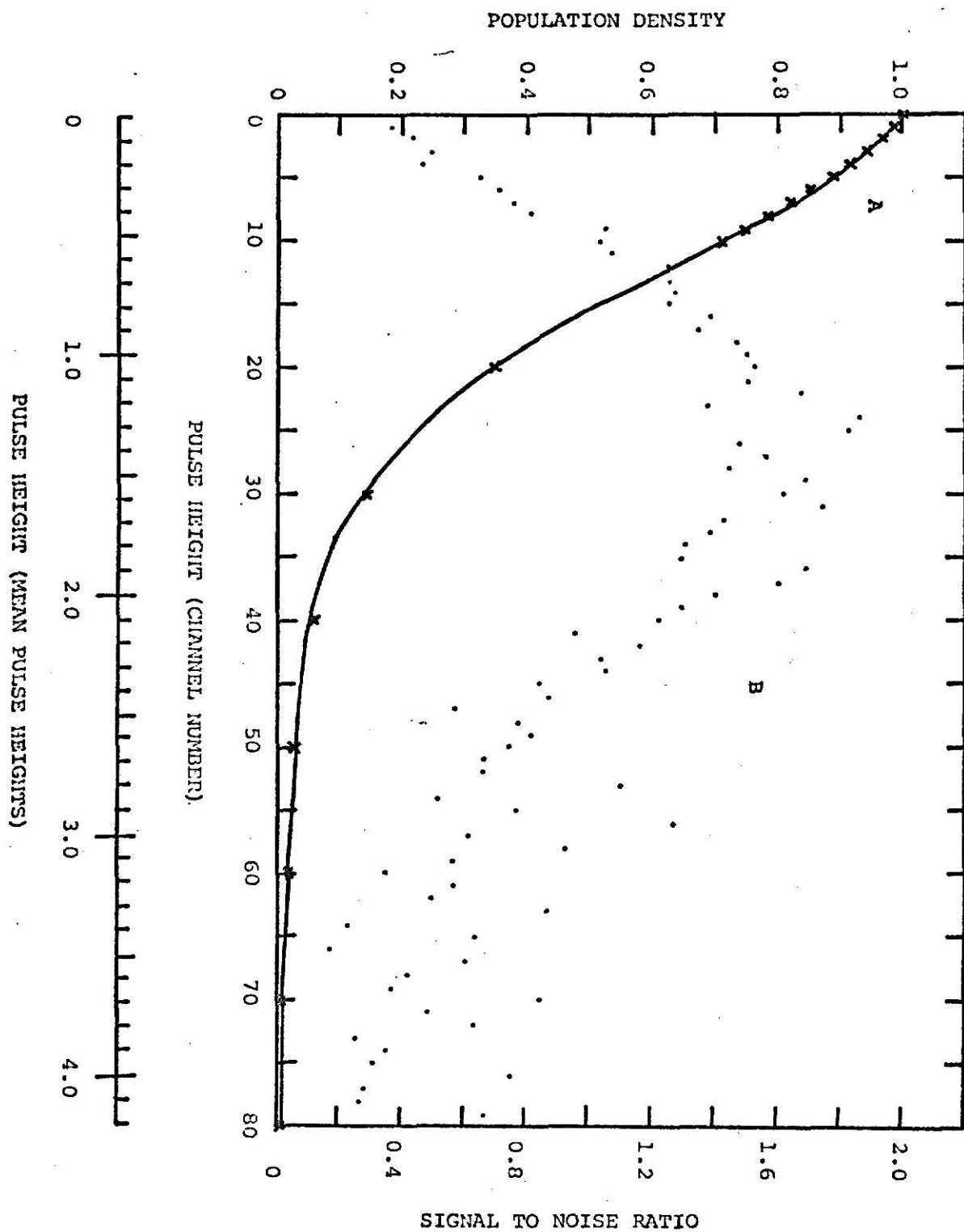


EXPLANATION OF PLATE XVII

These curves are for the R-106 operated at 1000 V, +22° C, runs 169-170.

- A. Curve A is the proportion of the single photoelectron pulse height distribution at or above a given channel. This is read on the left hand ordinate.
- B. Curve B is the ratio of the number of pulses in a given channel for a single photoelectron pulse height distribution to a dark noise pulse height distribution of equal total number of counts. This is read on the right hand ordinate.

PLATE XVII

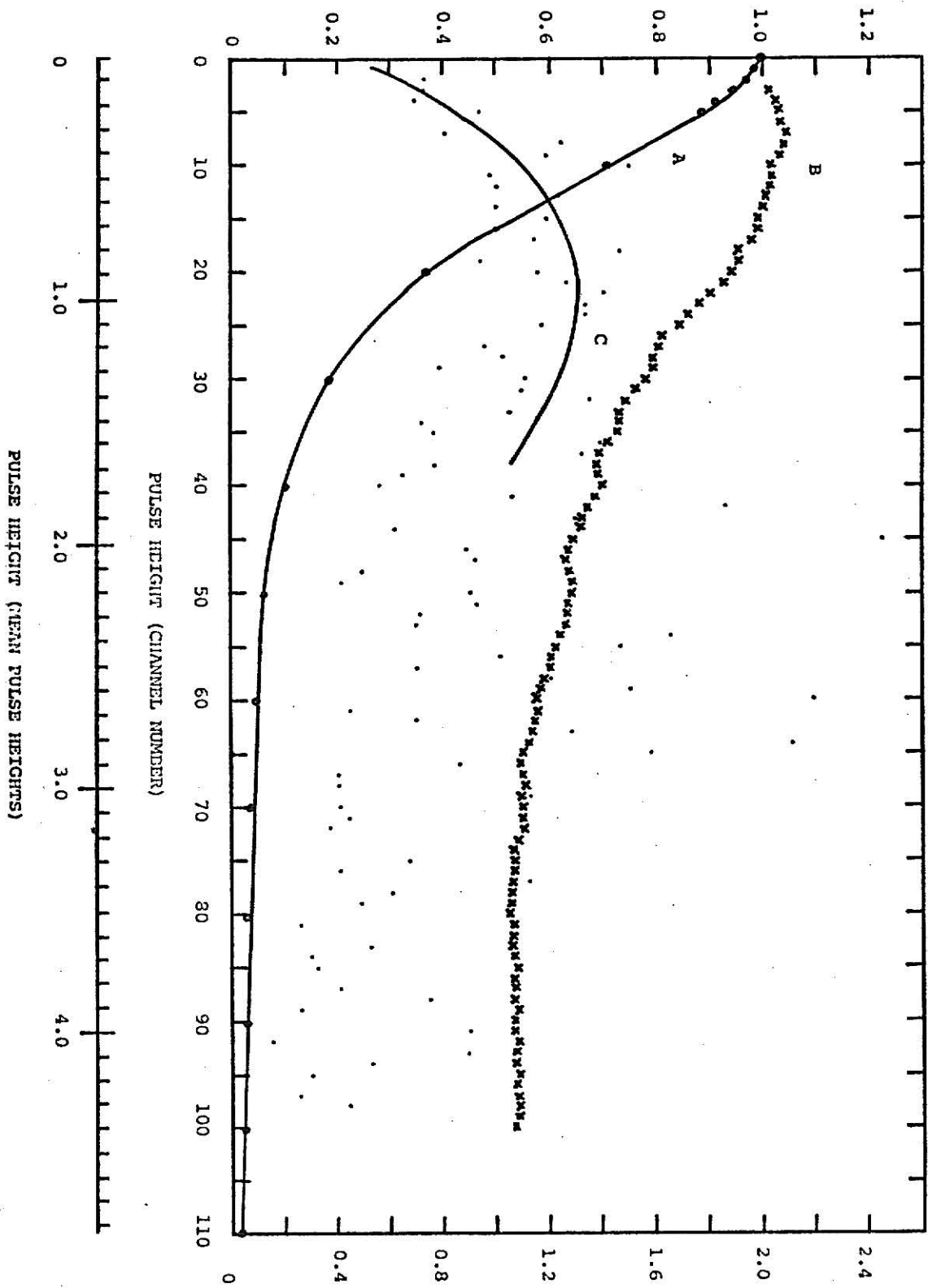


EXPLANATION OF PLATE XVIII

These curves are from the R-106, operated at 1005 V, -77° C, runs 175-176.

- A. Curve A is the total proportion of the single photoelectron pulse height distribution at or above a given channel. Curve A is read on the left hand ordinate.
- B. Curve B is the ratio of the single photoelectron and dark pulse populations at or above a given channel. Curve B is read on the left hand ordinate.
- C. Curve C is the ratio of the single photoelectron and dark pulse height populations of equal total number of counts. Curve C is read on the right hand ordinate.

PLATE XVIII

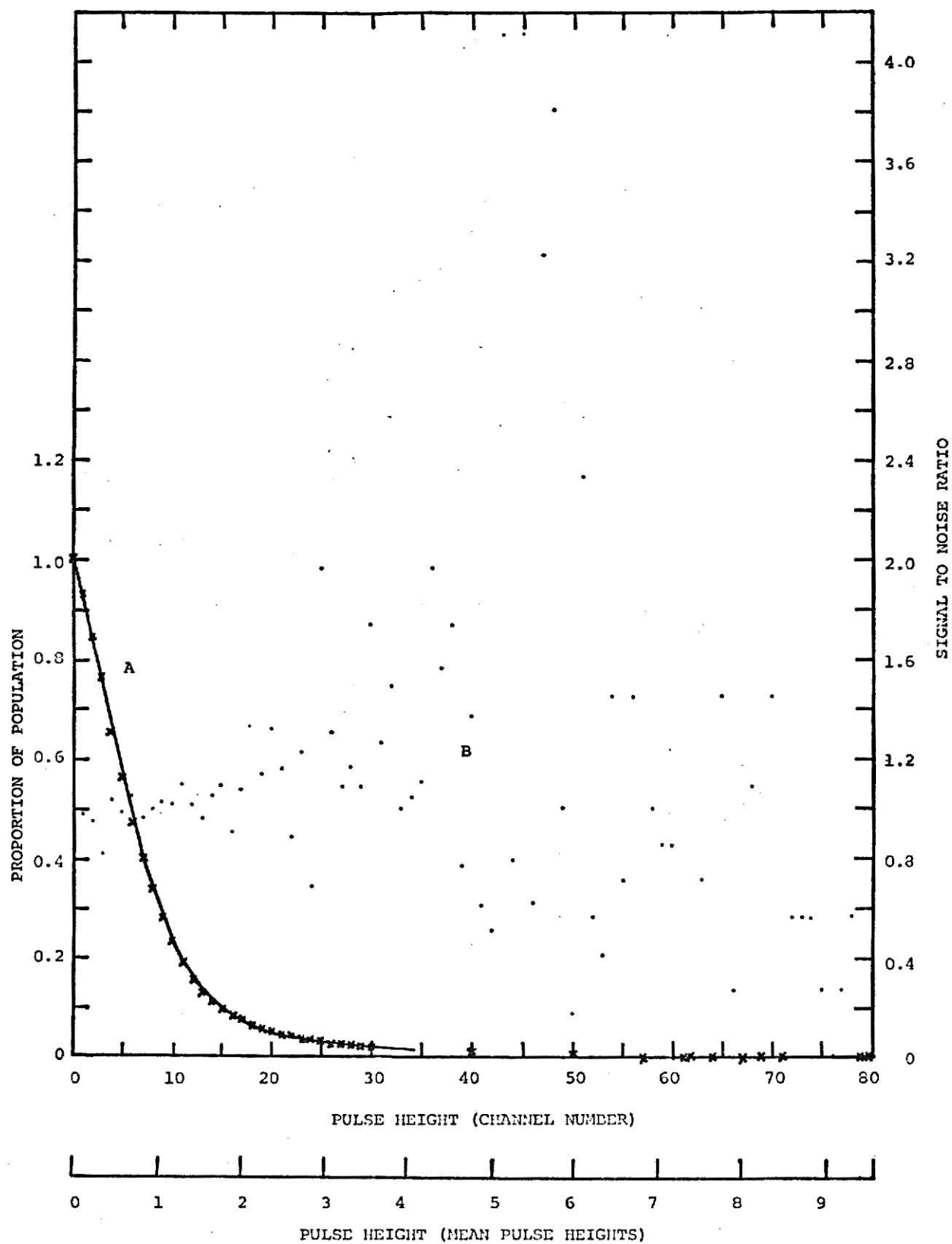


EXPLANATION OF PLATE XIX

These curves are from the R-106 run at 900 V at -73° C, run 174.

- A. Curve A is the proportion of the single photoelectron pulse height distribution at or above a given channel.
- B. Curve B is the ratio of the population of single photoelectron counts in a given channel to the dark pulse counts in that channel for signal and dark pulse populations of equal total size.

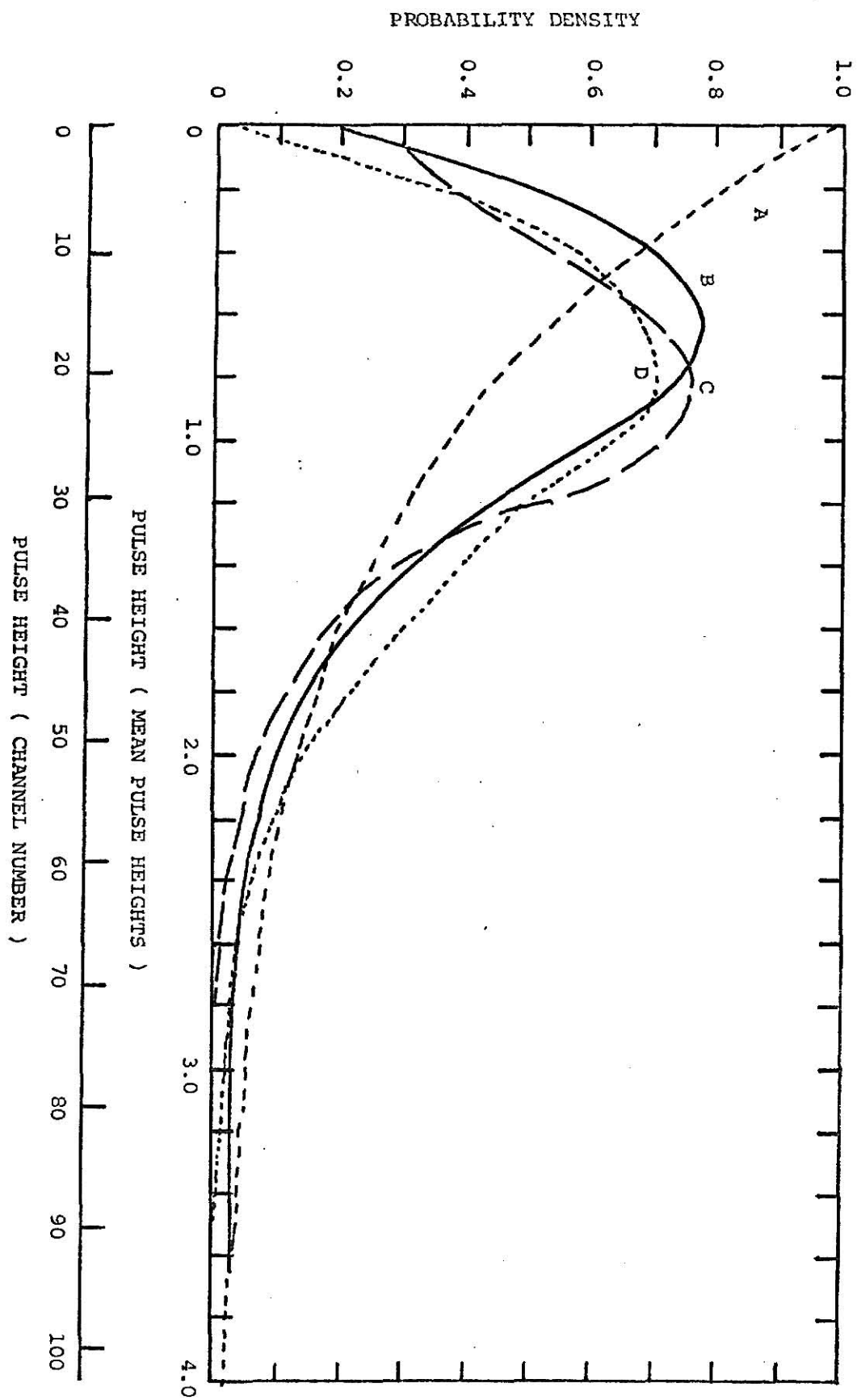
PLATE XIX



EXPLANATION OF PLATE XX

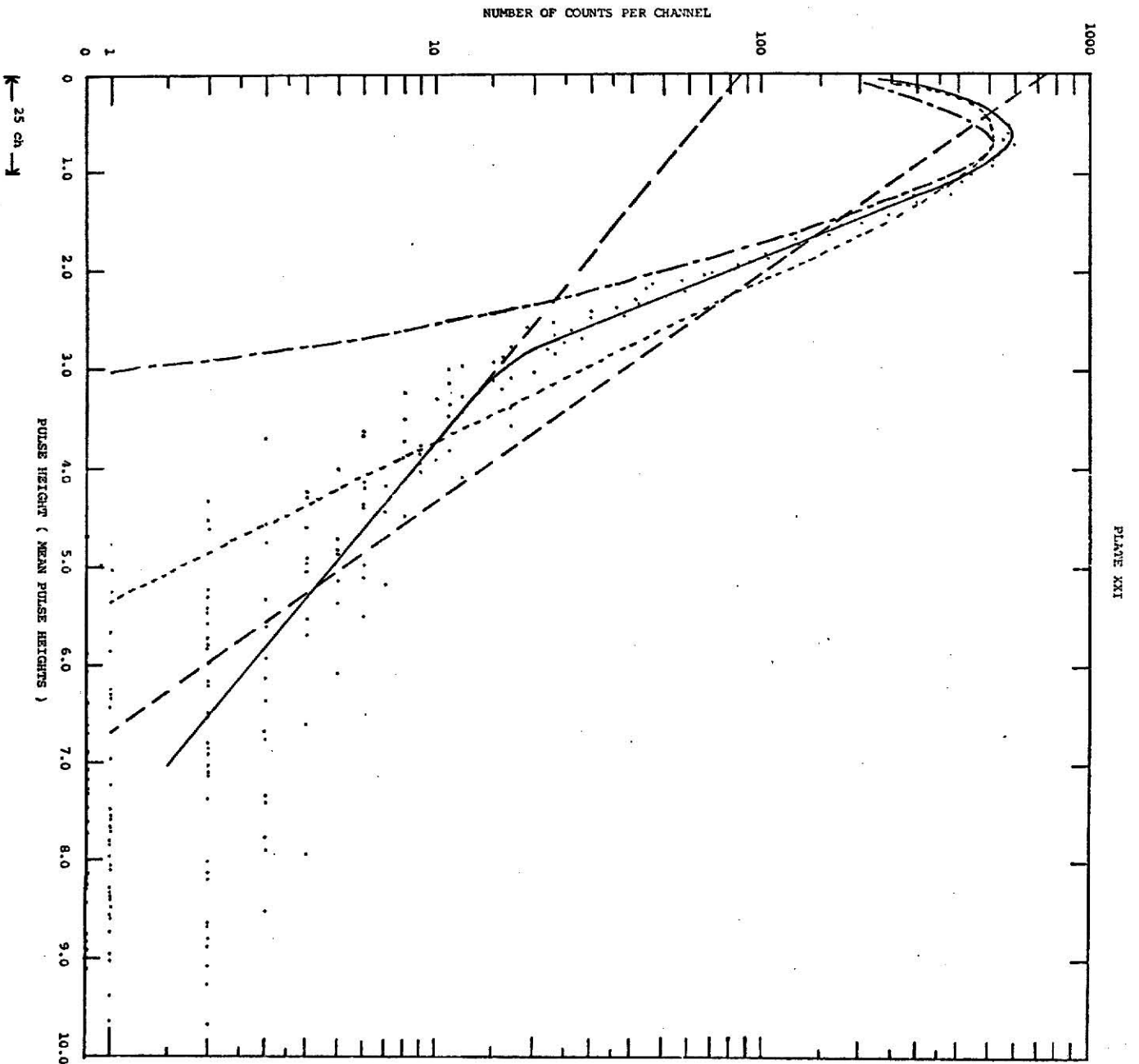
Single electron pulse height distribution for R-106 operated at 1100 V and -83° C, run 147. The dark pulse height spectrum has been subtracted. Superimposed are the calculated pulse height distributions from Prescott (1966) for $\mu = 5$, $b = .1, .2, .3$, and the single electron pulse height distribution less an exponential component.

PLATE XX



EXPLANATION OF PLATE XXI

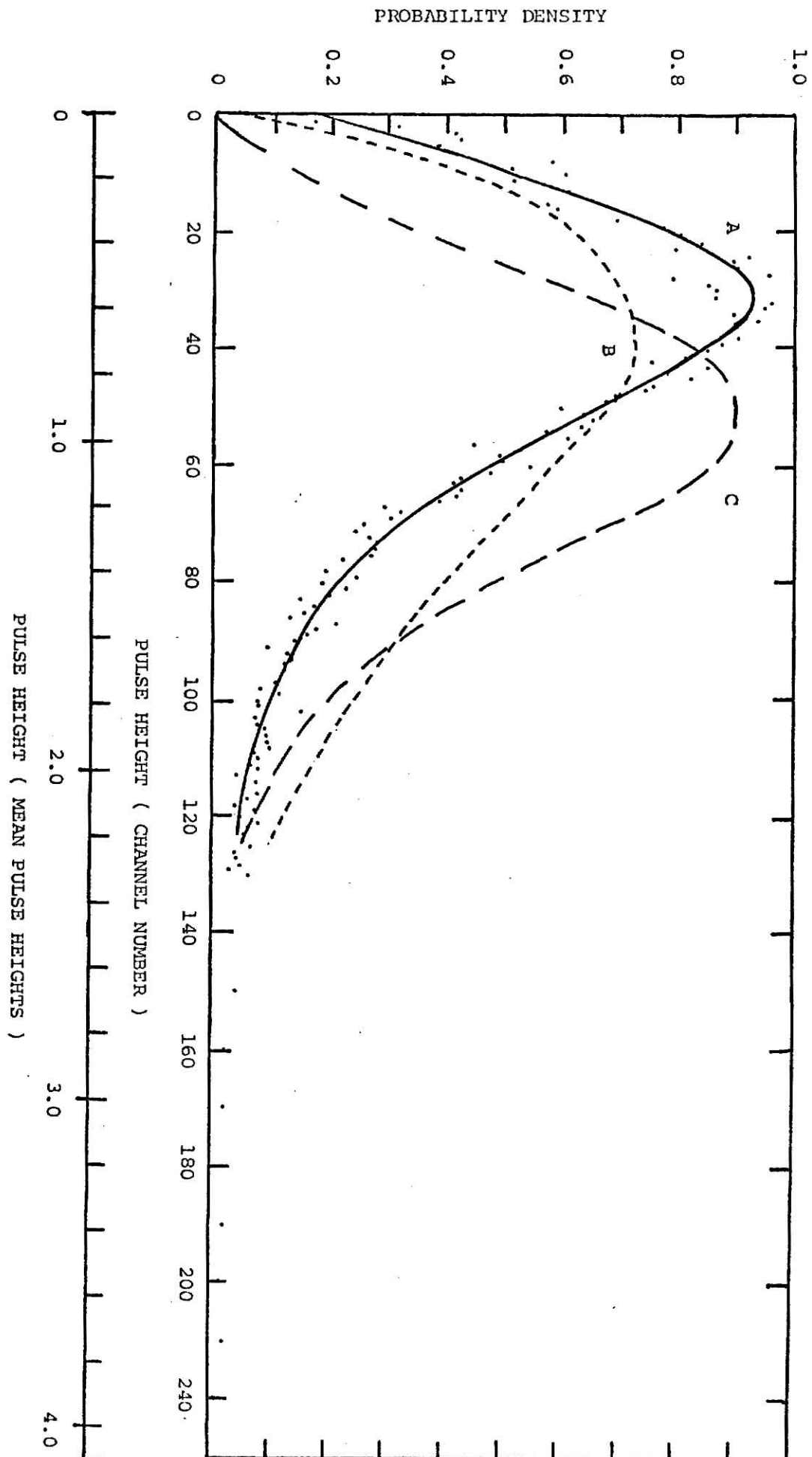
Curve C is the single electron pulse height distribution for R-106 at 1100 V, -83° C, run 147. The dark pulse height distribution has been subtracted. This distribution is not normalized. Superimposed are the distribution C less an exponential component, E, and the calculated distributions for $\mu = 5$, $b = .2$ (B) and $\mu = 5$, $b = 1.0$ (A).



EXPLANATION OF PLATE XXII

Curve A is the single electron pulse height distribution from R-106 operated at 1105 V, -77° C, run 179. Superimposed are the calculated distributions from Prescott (1966) for $\mu = 6$, $b = .2, 0$.

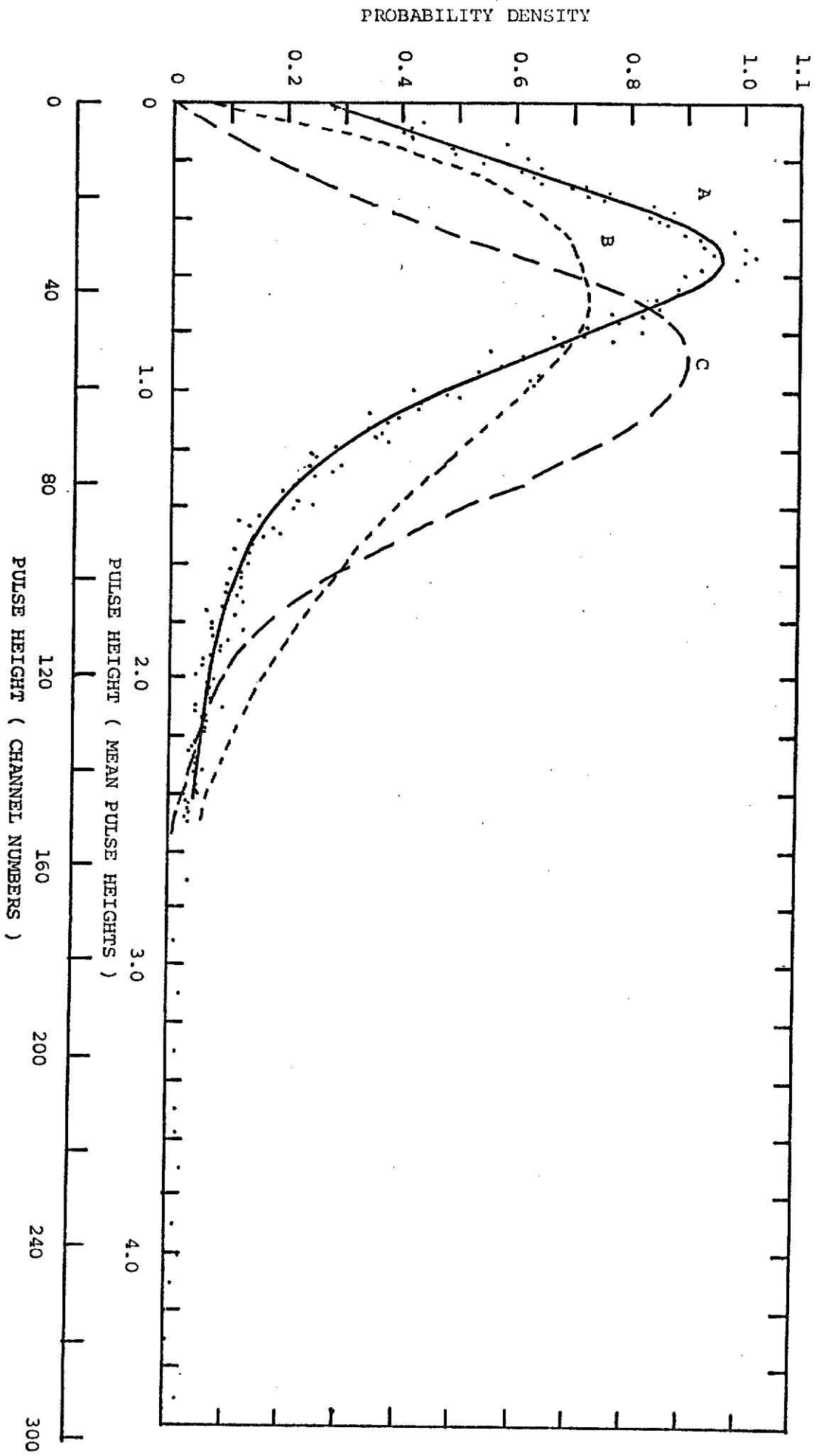
PLATE XXII



EXPLANATION OF PLATE XXIII

Curve A is the pulse height distribution for R-106 taken at 1100 V, -102° C, run 181. The dark pulse height distribution has been subtracted. Superimposed are the calculated pulse height distributions taken from Prescott's (1966) work with $\mu = 6$, $b = 0$ (C) and $\mu = 6$, $b = .2$ (B).

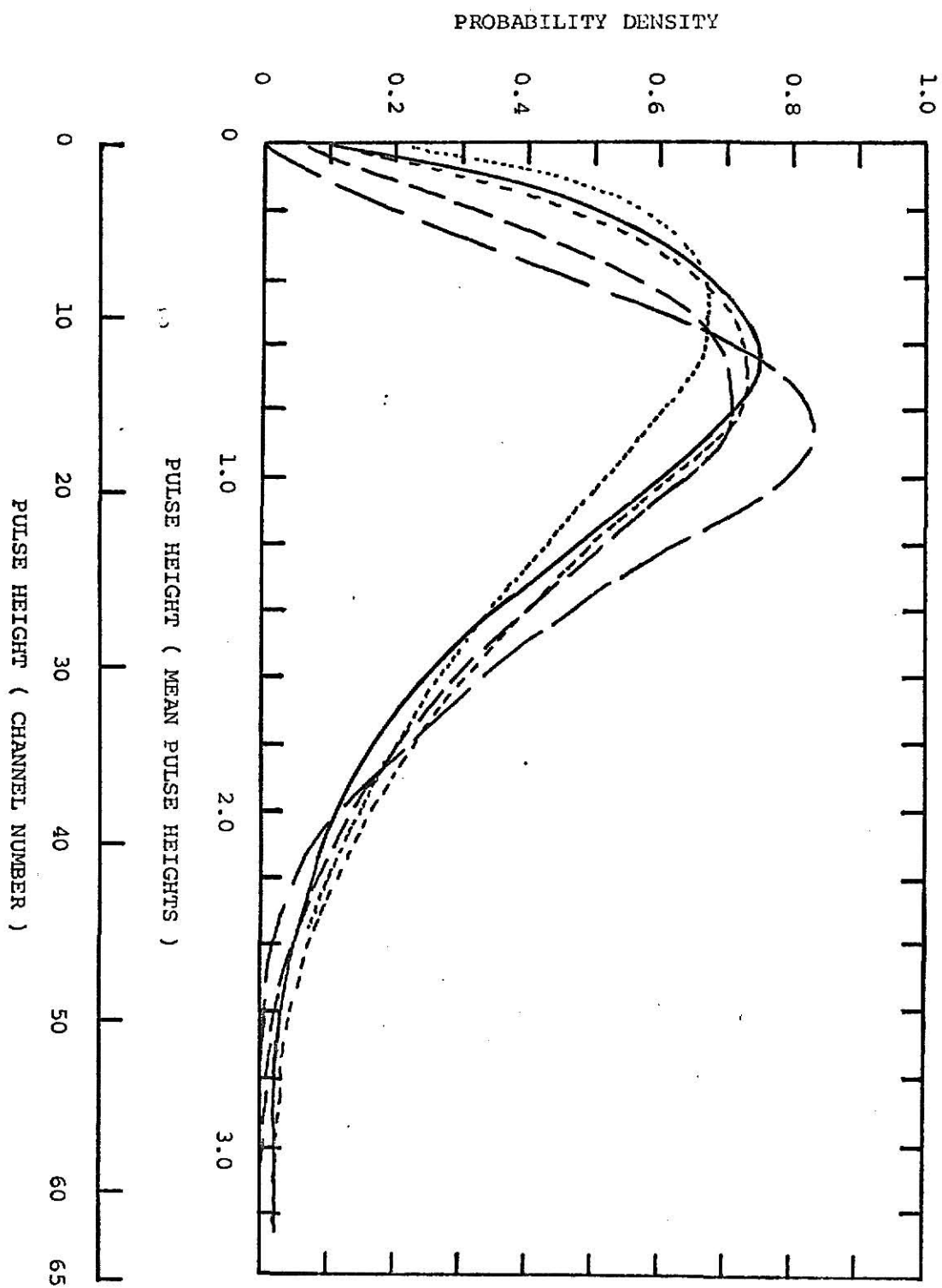
PLATE XXIII



EXPLANATION OF PLATE XXIV

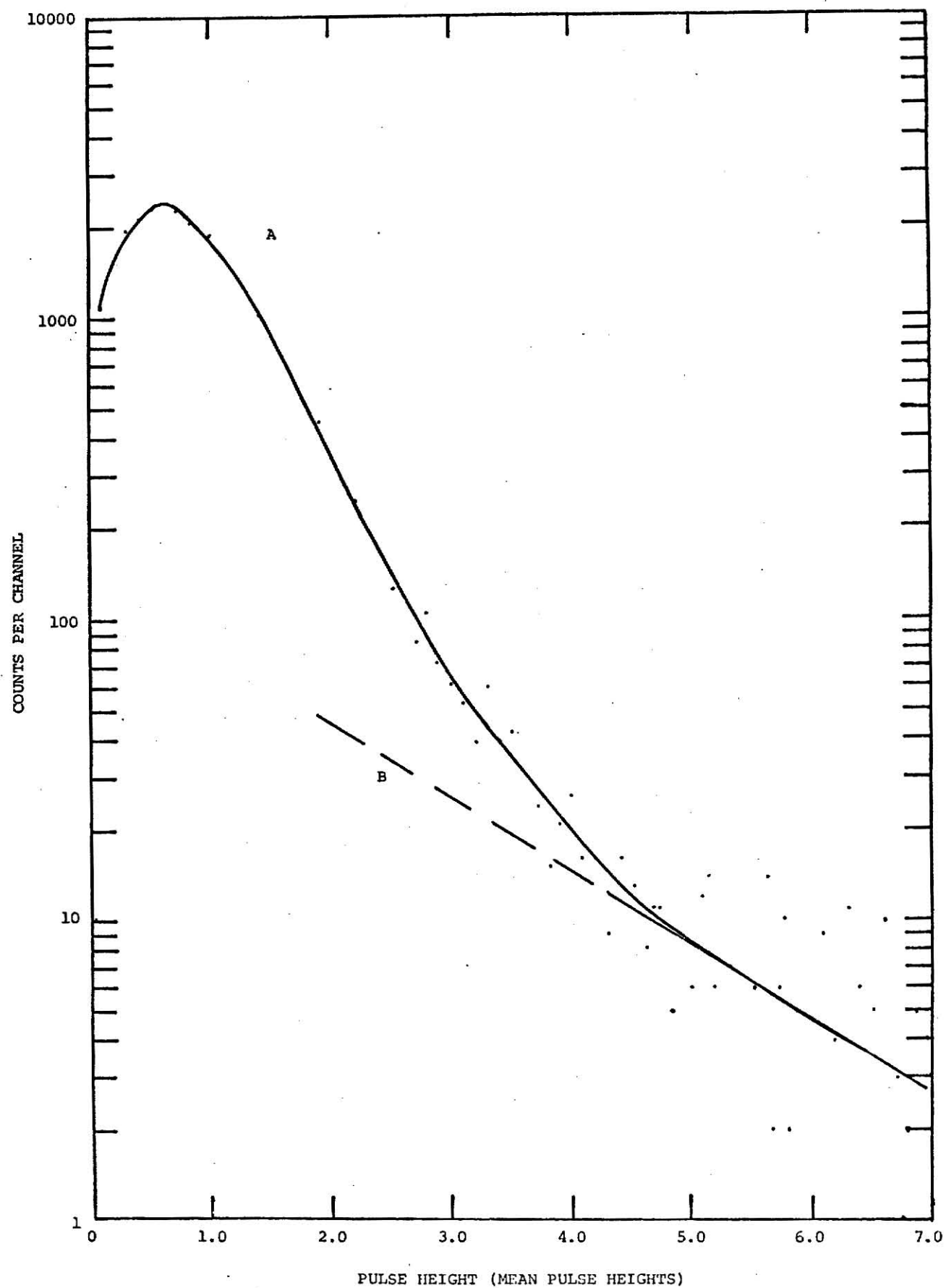
Pulse height distribution for 1000 V, +22° C, run 170. The dark counts have been subtracted. Superimposed are calculated pulse height distributions for $\mu = 5$, $b = 0, .1, .2, .3$ and $\mu = 6$, $b = .2$.

PLATE XXIV



EXPLANATION OF PLATE XXV

Single electron pulse height distribution for R-106 run at 1000 V, +22° C, run 170. Curve A is the single electron response and curve B is a possible exponential trend in curve A.



EXPLANATION OF PLATE XXVI

Fig. 1. Curve A is the single electron pulse height distribution for the R-106 run at -900 V, -73° C, run 174. The dark pulse height distribution has been subtracted. Superimposed is curve B, a running sum of $\sum_{i=1}^x i^2 f(i) = f(x)$. Curve A is read against the left ordinate, curve B against the right.

Fig. 2. Run 174 less an exponential component.

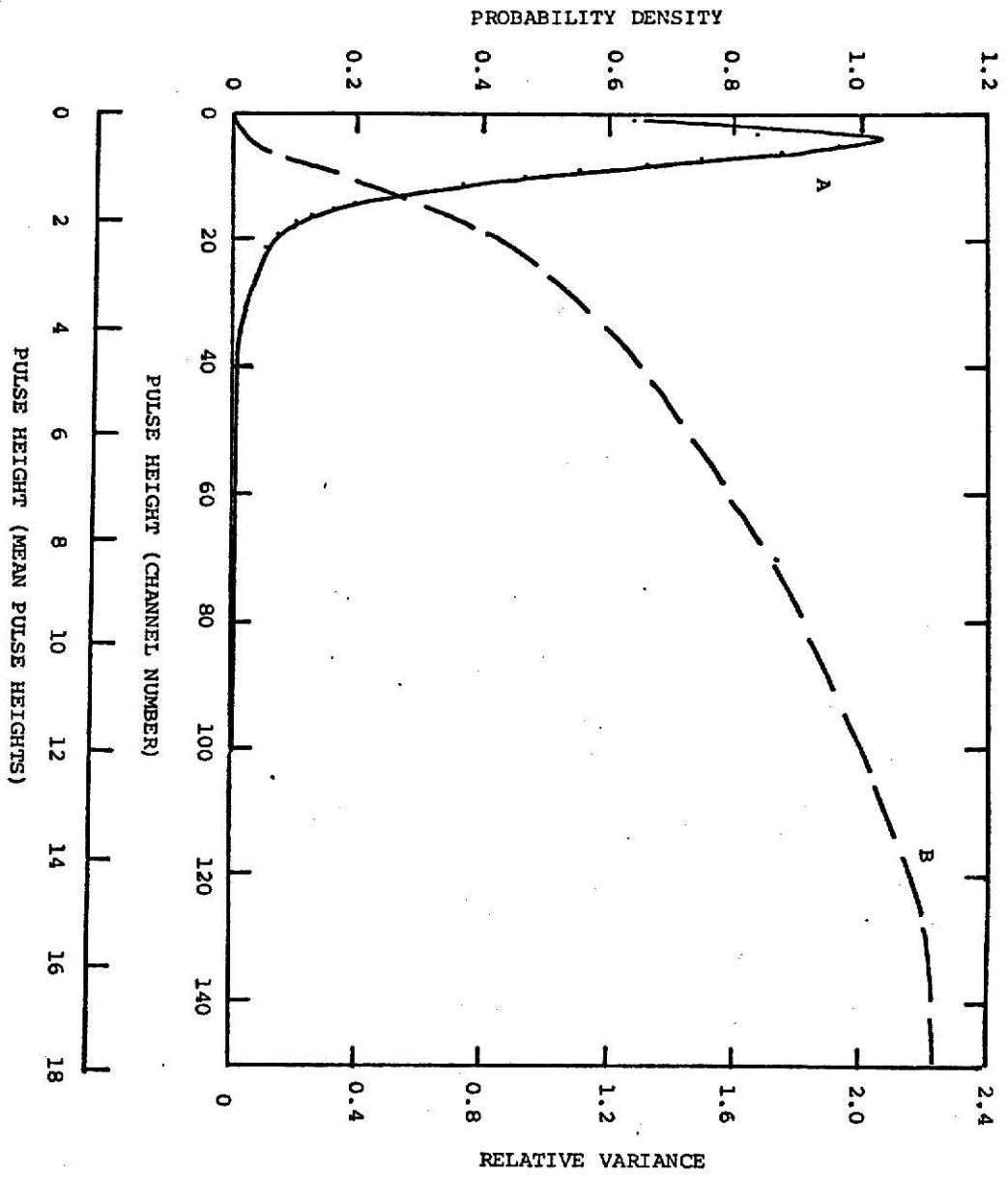


Figure 1.

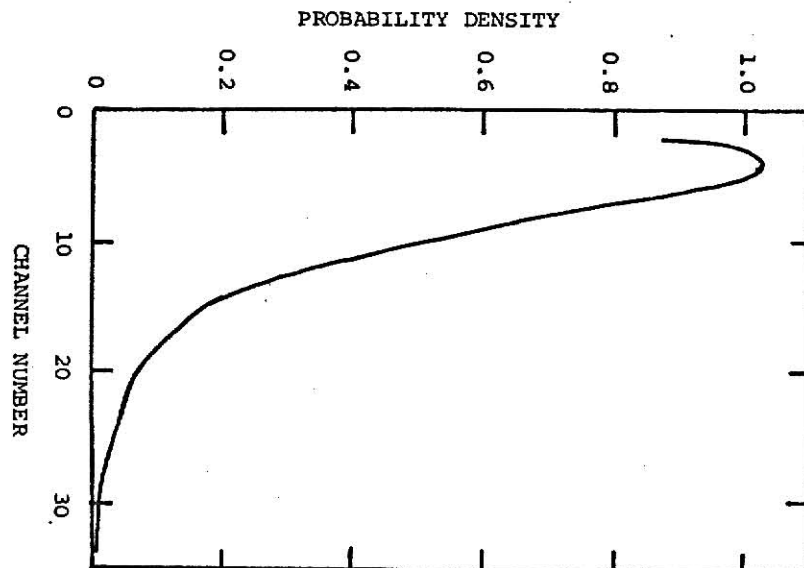
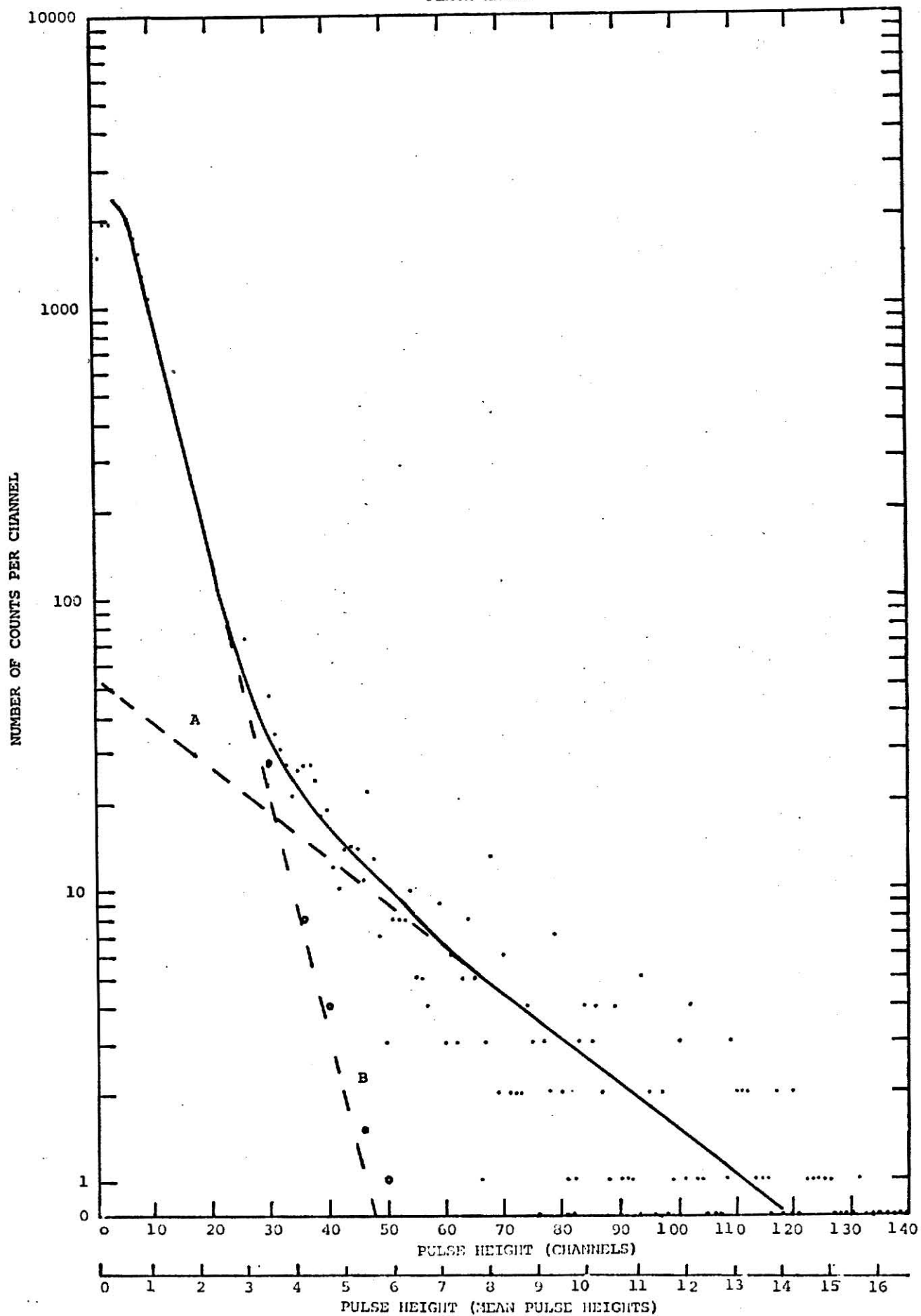


Figure 2.

EXPLANATION OF PLATE XXVII

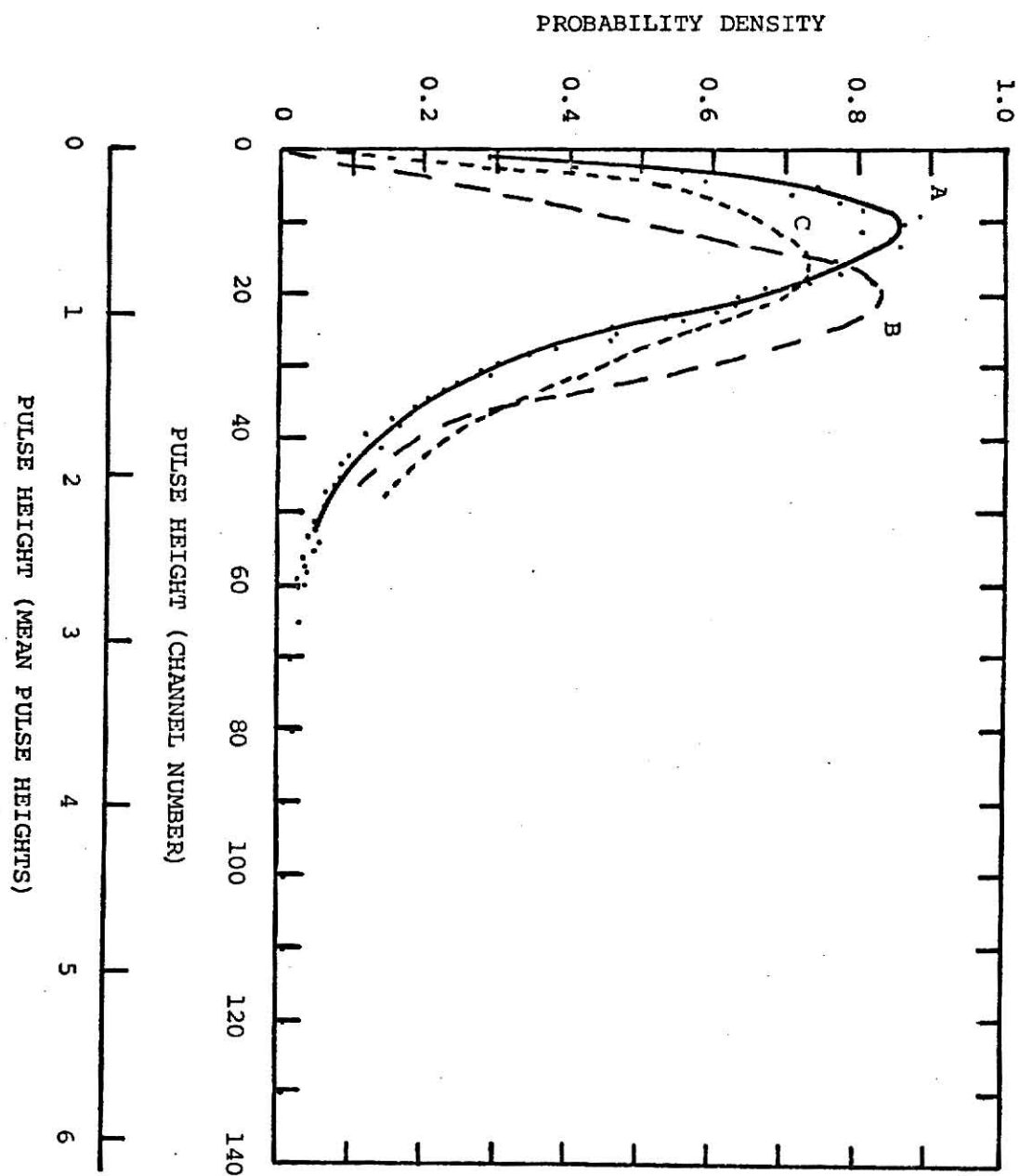
The solid line is the single electron pulse height distribution of the R-106 at 900 V, -73° C, run 174. The dark pulse height distribution has been subtracted. The dotted lines are (A) an exponential component and (B) the result of subtracting the exponential component.



EXPLANATION OF PLATE XXVIII

Curve A is the single electron pulse height distribution of R-106 at 1005 V, -77° C, run 176. Superimposed are the calculated distributions from Prescott (1966) for $\mu = 5$, $b = 0$ (curve B) and $\mu = 5$, $b = .2$ (curve C).

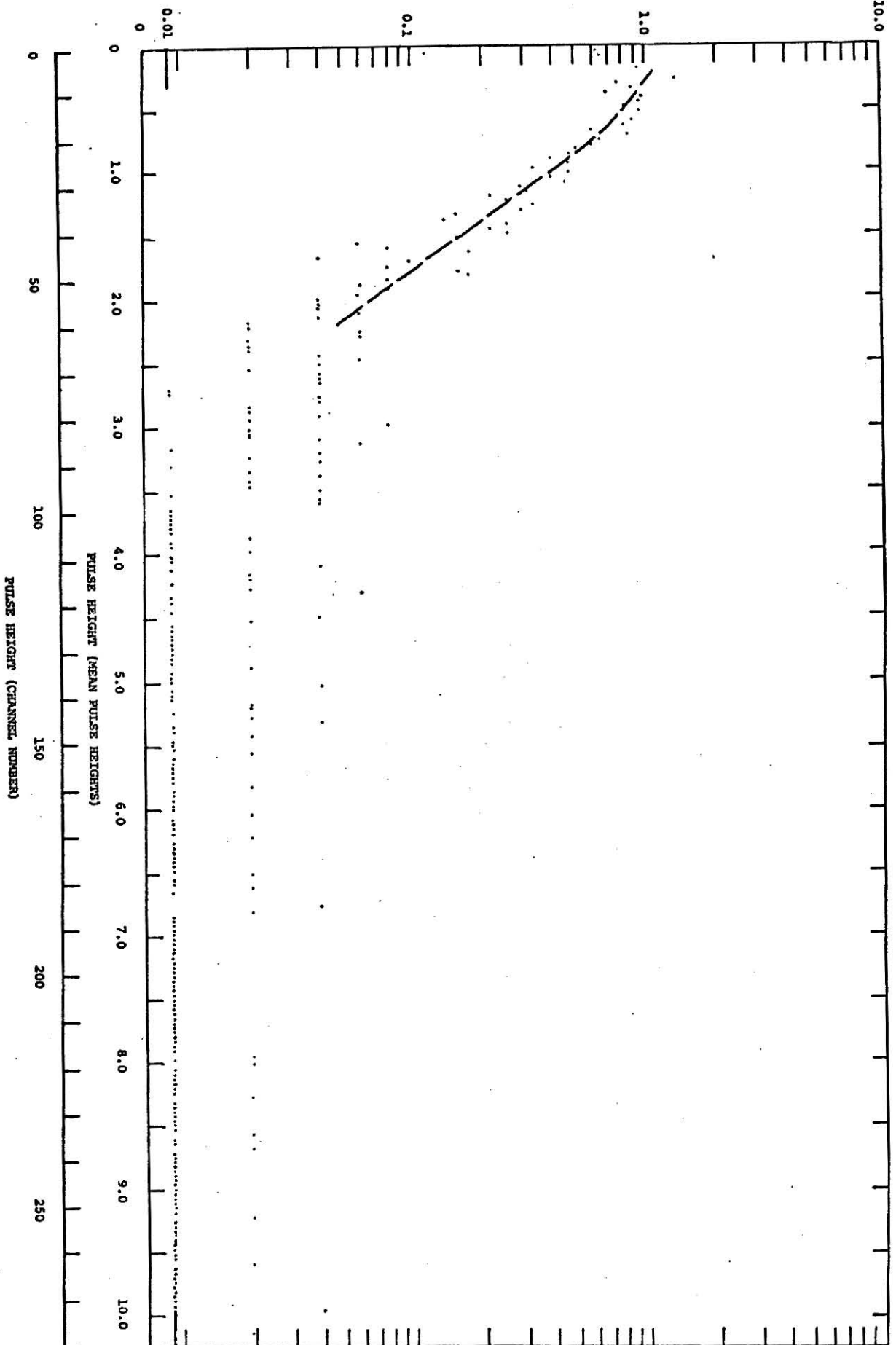
PLATE XXVIII



EXPLANATION OF PLATE XXIX

The dark pulse height distribution of the R-106 operated at 1005 V, -77° C, run 175. The data are truncated at a higher pulse height than others heretofore presented in order to show the high amplitude tail.

POPULATION DENSITY



APPENDIX

C FORMAT STATEMENTS

```

999 FORMAT(1H/1H , 9H BRAND JH/1H , 'PM TUBE DATA REDUCTION')
998 FORMAT(F5.0,2F10.0)
997 FORMAT(F10.0)
996 FORMAT(I5)
995 FORMAT(' PULSE HT',7X,'LIGHT',8X,'NORM. LITE',4X,'AT/ABV, LITE',2X
1,'AT/BELOW, LITE',4X,'S/N ABOVE',6X,'S/N BELOW',8X,'S/N',7X,'CHL')
994 FORMAT(' PULSE HT',7X,'DARK ',8X,'NORM. DARK',4X,'AT/ABV, DARK',2X
1,'AT/BELOW, DARK',10X,'CHL',5X,'DARK+LIGHT',5X,'LITE NORMII',4X,'D
2ARK NORMII')
993 FORMAT( F10.5,5X,F10.0,5X,F10.8,5X,F10.8,5X,F10.8,10X,F4.0,5X,F10.
13,2(5X,F10.8))
992 FORMAT(' MEAN OF LIGHT DIST. IS:',F10.5,' SUM IS:',F10.0,' REL.
1 VAR. IS:',F10.5)
991 FORMAT(' MEAN OF DARK DIST. IS:', F10.5,' SUM IS:',F10.0,' REL.
1 VAR. IS:',F10.5)
990 FORMAT(' VARIANCE AS RUNNING FUNCTION OF PULSE HEIGHT:')
989 FORMAT(4(5X,F10.6),5X,F10.0)
988 FORMAT(F10.0)
987 FORMAT( F10.5,5X,F10.0,5(5X,F10.8),5X,F10.7,2X,F4.0)
986 FORMAT(' CHL',5X,'LIGHT MEAN',5X,'DARK MEAN')
985 FORMAT(1X,F4.0,4X,F10.5,5X,F10.5)
    DIMENSION CUML(550),CUMD(550), ALITEN(550), DARKN(550)
    DIMENSION NCH(550),SNRA(550),SNRB(550),CRUD(550)
    DIMENSION ALITE(550), DLITE(550), DARK(550),SNRI(550)
    DIMENSION VARLTU(550), VARDKU(550),VARLT(550),VARDK(550)
    DIMENSION BCUML(550),BCUMD(550)
    DIMENSION PLSHTL(550),PLSHTD(550)
    DIMENSION CRAP(550),FILTH(550)
    REAL II
    REAL NCH
C     PROGRAM
C     AMEANL IS THE MEAN OF THE LIGHT DISTRIBUTION
C     AMEAND IS THE MEAN OF THE DARK DISTRIBUTION
C     VARLT AND VARDK ARE THE RELATIVE VARIANCES OF THE LIGHT AND DARK
C     DISTRIBUTIONS, RESPECTIVELY
C     SUML AND SUMD ARE THE SUMS OF ALL COUNTS IN THE TWO SPECTRA
    WRITE(3,999)
    1 READ(1,996,END=99) N
    READ(1,988) TIME
    SUML = 0.
    SUMD = 0.
    DO 100 I=1,N
    READ(1,998) NCH(I),DARK(I),CRUD(I)
    ALITE(I) = CRUD(I)-DARK(I)/TIME
    SUML = SUML+ALITE(I)
    SUMD = SUMD+DARK(I)
100 CONTINUE
    AMEAND = 0.
    AMEANL = 0.
    CUML(1) = 1.
    CUMD(1) = 1.
    ALITEN(1) = ALITE(1)/SUML
    DARKN(1) = DARK(1)/SUMD
    BCUML(1) = ALITEN(1)
    BCUMD(1) = DARKN(1)
    SNRA(1) = CUML(1)/CUMD(1)
    SNRB(1) = BCUML(1)/BCUMD(1)

```

```

SNRI(1) = ALITEN(1)/DARKN(1)
WRITE(3,986)
DO 200 I=2,N
  ALITEN(I) = ALITE(I)/SUML
  DARKN(I) = DARK(I)/SUMD
  CUML(I) = CUML(I-1)+ALITEN(I)
  CUMD(I) = CUMD(I-1)+DARKN(I)
  BCUML(I) = BCUML(I-1)+ALITEN(I)
  BCUMD(I) = BCUMD(I-1)+DARKN(I)
  SNRA(I) = CUML(I)/CUMD(I)
  SNRB(I) = BCUML(I)/BCUMD(I)
  IF( DARKN(I) .NE. 0. ) GO TO 150
  SNRI(I) = 100.
GO TO 160
150 SNRI(I) = ALITEN(I)/DARKN(I)
160 II = I
  AMEAND = DARKN(I)*II+AMEAND
  AMEANL = ALITEN(I)*II+AMEANL
  WRITE(3,985) NCH(I),AMEANL,AMEAND
200 CONTINUE
  VARDKU(I) = DARKN(I)
  VARLTU(I) = ALITEN(I)
  PLSHTL(I) = NCH(I)/AMEANL
  PLSHTD(I) = NCH(I)/AMEAND
  CRAP(I) = ALITEN(I)*AMEANL
  FILTH(I) = DARKN(I)*AMEAND
  WRITE(3,990)
  DO 250 I=2,N
    II = I
    VARLTU(I) = ALITEN(I)*II*II+VARLTU(I-1)
    VARDKU(I) = DARKN(I)*II*II+VARDKU(I-1)
    VARDK(I) = VARDKU(I)/AMEAND**2
    VARLT(I) = VARLTU(I)/AMEANL**2
    PLSHTL(I) = NCH(I)/AMEANL
    PLSHTD(I) = NCH(I)/AMEAND
    CRAP(I) = ALITEN(I)*AMEANL
    FILTH(I) = DARKN(I)*AMEAND
    WRITE(3,989) PLSHTL(I),VARLT(I),PLSHTD(I),VARDK(I),NCH(I)
250 CONTINUE
  WRITE(3,995)
  DO 300 I=1,N
    WRITE(3,987) PLSHTL(I),ALITE(I),ALITEN(I),CUML(I),BCUML(I),SNRA(I),
    1,SNRB(I),SNRI(I),NCH(I)
300 CONTINUE
  WRITE(3,994)
  DO 301 I=1,N
    WRITE(3,993) PLSHTD(I),DARK(I),DARKN(I),CUMD(I),BCUMD(I),NCH(I),
    1CRUD(I),CRAP(I),FILTH(I)
301 CONTINUE
  WRITE(3,992) AMEANL, SUML, VARLT(N)
  WRITE(3,991) AMEAND, SUMD, VARDK(N)
  GO TO 1
99 STOP
END

```


C FORMAT STATEMENTS

```

01 999 FORMAT(1H1/1H ,9H BRAND JH/1H ,14H PM STATISTICS)
02 998 FORMAT(2F10.0,2I10)
03 997 FORMAT(I5,9(2X,F10.8))
04 996 FORMAT(1H ,5H I ,9(12H P(K,I) ))
05 995 FORMAT(E14.7)
06 994 FORMAT(I5,10X,E14.7)
07 993 FORMAT(I5,3(10X,E14.7))
08 992 FORMAT(5H B= ,F10.8,5H M= ,F10.8,5H N= ,I5,5H L= ,I5)
09 991 FORMAT(9H SUM IS:)
10 990 FORMAT(14H I,P(K,I) ARE)
11 DIMENSION PSUM(9,1001),P1(9,1001),P2(9,1001),P(9,1001),SUM(9)
12 REAL M

C     PROGRAM
13 WRITE(3,999)
14 WRITE(3,991)
15 1 READ(1,998,END=99) B,M,N,L
C     CALCULATE PROBABILITY DENSITY
16 NN = N+1
17 P(1,1) = 0
18 P(1,2) = 1
19 DO 10 I=3,N
20 10 P(1,I) = 0
C     GET P(2,X)
21 DO 100 K=2,L
22 P1(K,1) = (1+B*M*(1-P(K-1,1)))
23 P2(K,1) = 1/P1(K,1)
C     X = 0
C     X = 1
C     IX = INTEGER X
24 IF(B .EQ. 0.) GO TO 7
25 B1 = -1./B
26 P(K,1) = P1(K,1)**B1
27 GO TO 8
28 7 P(K,1) = 0
29 8 X = 1
30 IX = 1
31 PSUM(K,2) = P(K,1)*P(K-1,2)
32 P(K,2) = M*P2(K,1)*PSUM(K,2)
C     X = 2 ONWARD
33 X = 2
34 SUM(K) = P(K,1)
35 DO 30 IX=2,N
36 PSUM(K,IX) = 0
37 DO 20 J=1,IX
38 PSUM(K,IX) = PSUM(K,IX) + P(K,J)*P(K-1,IX-J+2)*(X+(J-1.)*(E-1.))
39 20 CONTINUE
40 SUM(K) = SUM(K)+P(K,IX)
41 JJ = IX+1
42 LL = JJ
43 P(K,JJ) = (M/X)*P2(K,1)*PSUM(K,IX)
44 IF(P(K,JJ) .LE. .00000001) GO TO 110
45 X = X+1
46 30 CONTINUE
47 GO TO 130
48 110 DO 120 I=LL,N
49 120 P(K,I) = 0
50 130 WRITE(3,994) K,SUM(K)

```

```
51      100 CONTINUE
52      WRITE(3,992) B,M,N,L
53      WRITE(3,996)
54      DO 40 I=1,N
55      40 WRITE(3,997) I,P(1,I),P(2,I),P(3,I),P(4,I),P(5,I)
56      GO TO 1
57      99 STOP
58      END
```

ACKNOWLEDGMENTS

The author wishes to acknowledge and thank Dr. Basil Curnutte for his guidance and assistance in this study. He also wishes to thank Dr. C. L. Cocke for his advice and assistance with the electronics involved in this experiment and the National Science Foundation for their financial support during the course of this project.

REFERENCES

1. After Fig. 3(c), p. 6, An Introduction to the Photomultiplier, by EMI Corp.
2. R. L. Sproull, Modern Physics, (John Wiley and Sons, Inc., New York, 1963), 2nd ed., p. 464.
3. A. Rose, "Noise Currents", Photoelectric Materials and Devices, S. Larach ed., (D. Van Nostrand Co., Inc., Princeton, 1965), pp. 222-238.
4. G. T. Reynolds, "The Distribution of Single Electron Pulse Sizes from Multidynode Electron Multipliers and Single Electron Detection", Advances in Electronics and Electron Physics, vol. 22A (1966).
5. I. Pelchowitch, Rev. Sci. Inst. 26, 470 (1954).
6. R. L. Jerde, L. E. Petersen, and W. Stein, Rev. Sci. Inst. 38, 1387 (1967).
7. R. M. Matheson, IEEE Trans. Nucl. Sci. NS-11, 64 (1964).
8. A. Lallemand, "Photomultipliers", Astronomical Techniques, W. A. Hiltner ed., (The University of Chicago Press, Chicago, 1964), pp. 126-156.
9. E. H. Eberhardt, IEEE Trans. Nucl. Sci. NS-14, 7 (1967).
10. R. Alfano and N. Ockman, J. Opt. Soc. Am. 58, 90 (1968).
11. D. E. Persyk, Laser Journal 1, 21 (1969).
12. J. R. Prescott, Nucl. Inst. Meth. 22, 256 (1963).
13. R. Evrard and C. Gazier, J. Phys. 26, 37A (1965).
14. R. W. Engstrom, J. Opt. Soc. Am. 37, 420 (1947).
15. Z. Bay and G. Papp, IEEE Trans. Nucl. Sci. NS-11, 160 (1964).
16. Suggested by Dr. B. Curnutte.
17. J. A. Baiker, I.R.E. Trans. Nucl. Sci. NS-7, 74 (1960).
18. C. F. G. Delaney and P. W. Walton, Nucl. Inst. Meth. 25, 353 (1964).

19. M. Rome, Appl. Optics 5, 855 (1966).
20. G. C. Baldwin, S. I. Friedman, Rev. Sci. Inst. 36, 16 (1965).
21. F. J. Lombard and F. Martin, Rev. Sci. Inst. 32, 200 (1961).
22. G. A. Morton, Appl. Optics 7, 1 (1968).
23. M. Rome, Appl. Optics 5, 855 (1966).
24. E. H. Eberhardt, Appl. Optics 6, 251 (1967).
25. N. S. Khelebnikov, A. Ye. Melamid and T. A. Kovaleva, Rad. Eng. Elec. Phys. 7, 488 (1962).
26. R. F. Tusting, Q. A. Kerns, H. K. Knudsen, I.R.E. Trans. Nucl. Sci. NS-9, 118 (1962).
27. M. Bertolaccini and S. Cova, Energia Nucleare 10, 259 (1963).
28. M. Brault and C. Gazier, J. Phys. 24, 345 (1963).
29. L. G. Hyman, R. M. Schwarz, R. A. Schluter, Rev. Sci. Inst. 35, 393 (1964).
30. L. Coli, U. Facchini, A. Rossi, Nuovo Cim. 11, 255 (1954).
31. E. H. Eberhardt, IEEE Trans. Nucl. Sci. NS-11, 48 (1964).
32. G. Pietri, IEEE Trans. Nucl. Sci. NS-11, 76 (1964).
33. K. Haye, J. Phys. 23, 88 (1962).
34. L. Heroux, Appl. Optics 7, 235 (1968).
35. L. Janossy, Soviet Physics - J.E.T.P. 1, 520 (1955).
36. J. R. Prescott, Nucl. Inst. Meth. 39 (1966).
37. The following mathematics comes from Prescott (1966).
38. A. T. Young, Appl. Optics 2, 51 (1963).

PHOTOMULTIPLIER TUBE PARAMETERS
FOR MEASUREMENT OF LOW LIGHT LEVELS

by

JOHN HENRY BRAND II

B. S., Kansas State University, 1968

AN ABSTRACT OF A MASTER'S THESIS

submitted in partial fulfillment of the

requirements for the degree

MASTER OF SCIENCE

Department of Physics

KANSAS STATE UNIVERSITY
Manhattan, Kansas

1970

ABSTRACT

A cold box and system for delivering weak illumination to the photocathode of a Hamamatsu R-106 photomultiplier was constructed. The single electron pulse height distribution was measured with the weak illumination and a multichannel analyzer at temperatures from -102°C to room temperature. Back-biasing of the photocathode with respect to the first dynode apparently distorted the focus so that the single electron pulse height spectrum could not be obtained with that method. Based on a model of the electron multiplication process utilizing Polya statistics (Prescott, 1966), variances of the distribution were calculated for various values of interstage gain and a shaping parameter b , whose value determined whether the process followed exponential or Poisson probability rules. Curve fitting and matching of measured to theoretical variance indicated $b \sim .2$ and interstage gain $\sim 5 - 6$. Discriminator levels for optimizing signal-to-noise ratio in the pulse counting mode were determined.